AEDC-TR-83-2

c.4

A Steady-State Thermal Model for Analysis of Incipient Icing on an Airfoil Leading Edge

J. L. Fergus, Jr.
Sverdrup Technology, Inc.

July 1983

Final Report for Period January 1981 — September 1982

Approved for public release; distribution unlimited.

ARNOLD ENGINEERING DEVELOPMENT CENTER
ARNOLD AIR FORCE STATION, TENNESSEE
AIR FORCE SYSTEMS COMMAND
UNITED STATES AIR FORCE

NOTICES

When U. S. Government drawings, specifications, or other data are used for any purpose other than a definitely related Government procurement operation, the Government thereby incurs no responsibility nor any obligation whatsoever, and the fact that the government may have formulated, furnished, or in any way supplied the said drawings, specifications, or other data, is not to be regarded by implication or otherwise, or in any manner licensing the holder or any other person or corporation, or conveying any rights or permission to manufacture, use, or sell any patented invention that may in any way be related thereto.

Qualified users may obtain copies of this report from the Defense Technical Information Center.

References to named commercial products in this report are not to be considered in any sense as an endorsement of the product by the United States Air Force or the Government.

This report has been reviewed by the Office of Public Affairs (PA) and is releasable to the National Technical Information Service (NTIS). At NTIS, it will be available to the general public, including foreign nations.

APPROVAL STATEMENT

This report has been reviewed and approved.

Francis G. Araneo

FRANCIS G. ARANEO
Directorate of Propulsion Test
Deputy for Operations

Approved for publication:

FOR THE COMMANDER

Neil W Haars

NEIL W. HAARS, Colonel, USAF
Director of Propulsion Test
Deputy for Operations

UNCLASSIFIED

SECURITY CLASSIFICATION OF THIS PAGE *(When Data Entered)*

REPORT DOCUMENTATION PAGE		READ INSTRUCTIONS BEFORE COMPLETING FORM
1 REPORT NUMBER AEDC-TR-83-2	2 GOVT ACCESSION NO	3 RECIPIENT'S CATALOG NUMBER
4 TITLE *(and Subtitle)* A STEADY-STATE THERMAL MODEL FOR ANALYSIS OF INCIPIENT ICING ON AN AIR-FOIL LEADING EDGE		5 TYPE OF REPORT & PERIOD COVERED Final Report, January 1981 - September 1982 6 PERFORMING ORG REPORT NUMBER
7 AUTHOR(s) J. L. Fergus, Jr., Sverdrup Technology, Inc./AEDC Group		8 CONTRACT OR GRANT NUMBER(s)
9 PERFORMING ORGANIZATION NAME AND ADDRESS Arnold Engineering Development Center/DOT Air Force Systems Command Arnold Air Force Station, TN 37389		10 PROGRAM ELEMENT, PROJECT, TASK AREA & WORK UNIT NUMBERS Program Element 64361F
11 CONTROLLING OFFICE NAME AND ADDRESS Arnold Engineering Development Center/DOS Air Force Systems Command Arnold Air Force Station, TN 37389		12 REPORT DATE July 1983 13 NUMBER OF PAGES 67
14 MONITORING AGENCY NAME & ADDRESS*(if different from Controlling Office)*		15 SECURITY CLASS *(of this report)* UNCLASSIFIED 15a DECLASSIFICATION/DOWNGRADING SCHEDULE N/A

16 DISTRIBUTION STATEMENT *(of this Report)*

Approved for public release; distribution unlimited.

17 DISTRIBUTION STATEMENT *(of the abstract entered in Block 20, if different from Report)*

18. SUPPLEMENTARY NOTES

Available in Defense Technical Information Center (DTIC).

19 KEY WORDS *(Continue on reverse side if necessary and identify by block number)*

incipient icing
airfoil icing
thermal model

20 ABSTRACT *(Continue on reverse side if necessary and identify by block number)*

A steady-state thermal model was developed for analysis of incipient icing on the leading edge of wings, fins, or inlets of small missiles or drones at subsonic flight conditions. The model was found to be helpful in predicting the effects of liquid water content on the leading-edge surface temperature and on the free-stream static temperature and in interpreting incipient icing test results. Model description, model validation, model behavior, and examples of model applications are presented.

DD FORM 1 JAN 73 1473 EDITION OF 1 NOV 65 IS OBSOLETE

UNCLASSIFIED

SECURITY CLASSIFICATION OF THIS PAGE *(When Data Entered)*

PREFACE

The analysis reported herein was conducted by the Arnold Engineering Development Center (AEDC), Air Force Systems Command (AFSC), at the request of AEDC/DOP. The Air Force project manager was Mr. F. G. Araneo. The results were obtained by Sverdrup Technology, Inc., AEDC Group, operating contractor for Aeropropulsion Testing at the AEDC, AFSC, Arnold Air Force Station, Tennessee, under Project No. B312EH. Data analysis was completed on July 30, 1982, and the manuscript was submitted for publication on January 10, 1983.

The author wishes to acknowledge Dr. Jay D. Hunt, for consultant services during thermal model development, and Mr. J. M. Gallagher, for computer programming.

CONTENTS

Page

1.0 INTRODUCTION 7
2.0 MODEL DEVELOPMENT 7
2.1 Approach and Assumptions 7
2.2 Description 8
3.0 MODEL VALIDATION 13
3.1 Approach 13
3.2 Thermal Balance, Configuration A 15
3.3 Thermal Balance, Configuration B 18
3.4 Data Uncertainty 19
3.5 Summary 19
4.0 MODEL OUTPUT PARAMETER CHARACTERISTICS 20
4.1 Model Sensitivity 20
4.2 Heat Loss Audit 21
5.0 MODEL APPLICATIONS 21
5.1 Effects of Varying Liquid Water Content 22
5.2 Icing Onset Predictions 23
5.3 Anti-Icing Heater Sizing 24
5.4 Test Data Analysis 25
6.0 SUMMARY OF RESULTS 26
REFERENCES 27

ILLUSTRATIONS

Figure

1. Typical Leading-Edge System and Heat Balance Equation 29
2. Water Catch Efficiencies 31
3. Thermal Balance, Dry Air (Configuration A) 33
4. Calculated versus Measured Surface Temperature, Dry Air (Configuration A) 34
5. Difference Between Measured and Calculated Leading-Edge Surface Temperatures, Dry Air (Configuration A) 35
6. Thermal Balance, Wet Air (Configuration A) 36
7. Calculated versus Measured Surface Temperature, Wet Air (Configuration A) 37

Figure | Page

8. Thermal Balance, Model Adjusted, Wet Air (Configuration A) 38
9. Calculated versus Measured Surface Temperature, Model Adjusted, Wet Air (Configuration A) 39
10. Difference Between Measured and Calculated Leading-Edge Surface Temperatures, Model Adjusted,Wet Air (Configuration A) 40
11. Thermal Balance, Dry Air, QK = 0.0 (Configuration B) 41
12. Conduction Heat Loss as a Function of Structural Interface Temperature Gradient (Configuration B) 42
13. Thermal Balance, Dry Air, QK = f (DT) (Configuration B) 43
14. Calculated versus Measured Surface Temperature, Dry Air (Configuration B) 44
15. Difference Between Measured and Calculated Leading-Edge Surface Temperatures, Dry Air (Configuration B) 45
16. Thermal Balance, Wet Air (Configuration B) 46
17. Calculated versus Measured Surface Temperature, Wet Air (Configuration B) 47
18. Thermal Balance, Model Adjusted, Wet Air (Configuration B) 48
19. Calculated versus Measured Surface Temperature, Model Adjusted, Wet Air (Configuration B) 49
20. Difference Between Measured and Calculated Leading-Edge Surface Temperatures, Model Adjusted, Wet Air (Configuration B) 50
21. Sensitivity of Output Parameters for a One-Percent Increase in Input Parameters 51
22. Sensitivity of QNET for a One-Percent Increase in Input Parameters 52
23. Typical Heat Loss Audit as a Function of Liquid Water Content 53
24. Effect of Liquid Water Content on Leading-Edge Surface Temperature 54
25. Effect of Liquid Water Content on Free-Stream Static Temperature 56

Figure | Page

26. Icing Onset Predictions, Isolated Airfoil (Configuration B) 58
27. Comparison of Icing Onset Predictions and Test Results (Configuration B) 59
28. Effect of Heater on Reducing Icing Onset Temperature 60
29. Surface Temperature and Power Density Required for Dry Anti-Icing 61

TABLES

1. Uncertainties of Calculated Data 62
2. Model Sensitivity for a One-Percent Increase in Input Parameters 63

NOMENCLATURE 65

1.0 INTRODUCTION

After an icing test conducted in the Arnold Engineering Development Center (AEDC) Engine Test Facility in 1980, a study was initiated to obtain a better understanding of the environmental conditions conducive to incipient icing on the leading edge of an airfoil. The primary result was the development of a steady-state thermal model for analyzing the leading edges of wings, fins, or inlets of small missiles or drones at subsonic flight conditions. The model was found to be helpful in predicting the effects of liquid water content (LWC) on the leading-edge surface temperature and the free-stream static temperature and in analyzing incipient icing test results.

The purpose of this report is to present a description of the thermal model, the model validation, a discussion of the model behavior, and examples of model applications.

2.0 MODEL DEVELOPMENT

2.1 APPROACH AND ASSUMPTIONS

The approach was to design a steady-state model for subsequent trimming and validation based on experimental or test results. After validation of the steady-state model, further development can be effected to improve the model capability for addressing a wider range of conditions and time-dependent input parameters.

Consistent with this approach, three basic assumptions were made for the initial model. First, the thermal model was designed for steady-state conditions, i.e., when thermal equilibrium has been established. In flight this is not the case for incipient icing during the first few minutes after entry into an icing cloud, when the airfoil temperature is changing, but it is the case after the temperature has stabilized. Therefore, one needs to exercise care in interpreting the model results when using test or experimental data as inputs. Often the time-dependent changes in test conditions are sufficiently small to permit the calculation of useful information. Second, the model does not account for ice accretion. Finally, the leading-edge shape was chosen to be represented by a half cylinder because this configuration approximates typical leading-edge shapes and because water catch efficiency and forced convection heat-transfer coefficient data for a cylinder are readily available.

Other assumptions and considerations will be discussed in this section and subsequent sections of this report.

2.2 DESCRIPTION

The thermal model is a heat balance of the leading edge. Based on the conservation of energy, the terms of the heat balance equation proffered by Messinger (Ref. 1) and Schultz and Willbanks (Ref. 2) were used:

$$\begin{aligned} QNET &= \text{Heat Loss} - \text{Heat Gain} \\ &= \Sigma_{loss}\,[QC\ (\text{Convective}), QE\ (\text{Evaporative}), QS\ (\text{Sensible})] \\ &\quad - \Sigma_{gain}\,[QF\ (\text{Air Kinetic Energy}), QKE\ (\text{Water Kinetic Energy})] \end{aligned}$$

To this heat balance, two terms were added: (1) a heat loss term (QK, Conduction) to account for conduction heat loss at the aft structural interface, and (2) a heat gain term (PA, Heater Power Density) to account for an anti-icing heater. These heat-transfer modes are shown schematically in Fig. 1. The basic thermal balance equation (per unit area) is:

$$\begin{aligned} QNET = {} & HC(TS - T0) + MPR(M/A)L + (M/A)(CW)(TS - T0) + QK \\ & - HC(R)V^2/2GJ(CA) - (M/A)V^2/2GJ - PA,\ \text{Btu/hr-ft}^2 \end{aligned}$$

where

A = Leading-edge area, ft^2

CA = Specific heat at constant pressure for air, 0.24 Btu/lbm-°F

CW = Specific heat of water, 1.0 Btu/lbm-°F

G = Constant, 32.174 lbm-ft/lbf-sec^2

HC = Calculated convective heat-transfer coefficient, Btu/hr-ft^2-°F

J = Mechanical equivalent of heat, 778 ft-lbf/Btu

L = Latent heat of vaporization for water, 1,060 Btu/lbm

M = Rate of water catch, lbm/hr

MPR = Fraction of water evaporated

PA = Heater power density, Btu/hr-ft^2

QK = Aft conductivity, Btu/hr-ft^2

R = Boundary-layer recovery factor, 0.875 average for laminar and turbulent flow (Ref. 1). (Use the appropriate value(s) based on the local flow conditions.)

T0 = Free-stream static temperature, °F, °R

TS = Leading-edge surface (skin) temperature, °F, °R

V = Free-stream velocity, ft/sec

References 1 and 2 do not include the equations for calculating HC and M, (1) and (2) below. The following equation for HC was obtained from Ref. 3:

$$HC = 0.194(TF)^{0.49}\,[V(RHO)/D]^{0.50}\,(1 - |\theta/90|^3),\ \text{Btu/hr-ft}^2\text{-°F} \qquad (1)$$

where

TF = 0.5 (TS + T0), °R

RHO = Free-stream air density, P0/R(TF), lbm/ft^3

D = Effective diameter of leading edge, ft (See Fig. 1)

θ = Included angle between point on surface and stagnation point, integrated from 0 to 90 deg to obtain an average value over the leading edge.

(An alternate equation for HC, from Ref. 4, was used for verification:

$$HC = (0.855)\,(K/D)\,(27{,}798.336\ MU/K)^{0.4}\,[V(D)RHO/(MU)G]^{0.5},\ \text{Btu/hr-ft}^2\text{-°F}$$

where

K = Conduction heat-transfer coefficient for air in the boundary layer
= $0.001533\ TFK^{1.5}/(TFK + 245.4 \times 10^{-12/TFK})$, Btu/hr-ft-°F (Ref. 5)
(TFK = TF, °K),

and

MU = Viscosity of air in boundary layer
= lbf-sec/ft^2, calculated using
Sutherland's equation.

Agreement within ±1.1 percent was obtained.)

$$M = 0.38(VK)D(LWC)E(S),\ \text{lbm/hr} \qquad (2)$$

where

VK = Velocity, kts

LWC = Liquid water content, gm/m^3

E = Water catch efficiency.

Excluding the S term, the aforementioned equation for M as obtained from Refs. 4 and 6 gives the water catch rate per foot of airfoil span. The S term was added to account for the total span in feet.

The water catch efficiency, E, is the ratio of the water intercepted (impinged on the leading edge) to the amount of water contained in the cloud streamtube which flows over the leading edge. It is a function of the modified inertia parameter, K0, which accounts for water droplet inertia. K0 is calculated from the expression given in Ref. 4 (accurate within ± 5 percent, per Ref. 6):

$$K0 = 1.87 \times 10^{-7} [1.15\ VK/(MU)G]^{0.6}\ DD^{1.6}/12\ D(RHO)^{0.4}$$

where

DD = Volume median droplet diam, μ.

Water catch efficiency is determined from a graph of E as a function of K0 for a cylinder as obtained from Ref. 6. This relationship is shown in Fig. 2 in addition to that for other aerodynamic configurations.

The next term in the thermal balance to be defined is the evaporation fraction, MPR, the ratio of the amount of water evaporated from the surface to the amount of water intercepted by the surface, or

$$MPR = EP/(M/A)$$

where

EP = Evaporation potential, for this analysis the potential or maximum amount of water per unit area that can be evaporated, a function of the difference between the water vapor pressure based on the surface (leading edge) temperature and the vapor pressure based on the free-stream static temperature.

The intercepted water is subject to three processes: freezing, being windswept along the surface (runback), and evaporation. In this analysis, no provisions are made to account for freezing or ice accretion. Therefore, only complete evaporation or partial evaporation and partial runback can occur. Complete evaporation can be effected only at relatively high surface temperatures, generally above 100°F for the usual cloud encounters. Therefore, the more common condition is partial evaporation of the intercepted water with attendant runback of the remainder. However, the partial evaporation in this model is the maximum

that can be potentially evaporated based on the two vapor pressures previously defined. This is the general approach used by Messinger, and

$$EP = KM\,(HC)\,(PTSW - PT0W)/P0,\ lbm/hr\text{-}ft^2$$

where

P0 = Free-stream static (ambient or atmospheric) pressure, psia

PTSW = Water vapor pressure at the surface temperature, TS. For TS > 32°F, PTSW was obtained from a curve fit of vapor pressure as a function of temperature from steam tables (Ref. 7).

PT0W = Water vapor pressure at T0, i.e., free-stream (atmospheric) vapor pressure of the water droplets, psia. This assumes that the water droplet temperature is the same as the free-stream static temperature. For T0 < 32°F, the following expression was used for PT0W (Refs. 2 and 8):

$$PT0W = 14.696 \exp\{2.3\,[A1 + B1/T + C1(T^2 - K)/T\,[10^{D1(T^2-K)^2} - 1.0] + E1\,[10^{F1(374.11-T)^{5/4}}]]\},\ psia$$

where

$$T = (T0 + 459.67)/1.8,\ °K$$

and

$A1 = 5.4266514$ $\quad D1 = 1.1965 \times 10^{-11}$ $\quad K = 2.937 \times 10^5$

$B1 = -2005.1$ $\quad E1 = -4.4 \times 10^{-3}$

$C1 = 1.3869 \times 10^4$ $\quad F1 = -5.7148 \times 10^{-3}$

For T0 >32°F, PT0W was obtained from a curve fit of vapor pressure as a function of temperature from steam tables (Ref. 7).

Referring to the EP equation, KM according to Messinger is a constant, 2.9. Sogin (Ref. 9) derives it from the expression $0.622\ I/CA = 2.90$, i.e., where $I = (PR/SC)^{0.67} = 1.12$ and states that it is based on the assumption of laminar mass transfer, the mass transfer from the surface to the free stream. Sogin further states that KM = 2.6 if the mass transfer is turbulent (I = 1.0). He includes other estimates of I by many investigators for the reader's perusal. In this model KM is calculated for each environmental condition using the expression

$$KM = (0.622/CA)\,(PR/SC)^{0.67},\ lbm\text{-}°F/Btu$$

where

$$PR = 3600(G)CA(MU)/K = 27798.336\ MU/K$$

and

$$SC = MU/RHO(DF)$$

where

$$DF = 0.000146\ TF^{2.5}/[(TF + 441)(PO/14.696)],\ ft^2/hr \quad \text{(Ref. 10)}$$

KM was evaluated for a set of 72 data points and varied from 2.8602 to 2.8686 (I = 1.104 to 1.107).

The ratio EP/(M/A) or MPR is an indicator of the amount of runback. When EP = M/A,

MPR = 1.0 (no runback, all intercepted water is evaporated).

When EP < M/A,

MPR = EP/(M/A). (M/A − EP = unit runback).

Referring again to the EP equation, some authors include an additional term called the "wettedness" factor, particularly for analyzing the wing areas *aft* of the leading edge. This factor is the ratio of the wetted surface area to the total area. For the leading edge, the wettedness factor is generally assumed to be unity. Such is the case in this model. The reader is cautioned to use a value appropriate to the particular conditions/configuration being investigated.

The heat gain (QG) and the heat loss (QL) are calculated as follows:

$$QG = QF + QKE + PA,\ w/in.^2$$

$$QL = QC + QE + QS + QK,\ w/in.^2$$

where all of the component terms are converted from Btu/hr – ft^2 to w/$in.^2$ by the factor 2.0353×10^{-3}.

$$QNET = QG - QL, \text{ w/in.}^2$$

The units w/$in.^2$ are used because they are the commonly used units for describing the heater capacity or the heater power density.

3.0 MODEL VALIDATION

3.1 APPROACH

The model validation consisted of inputting measured test data to the thermal model, examining the degree of thermal balance achieved, and then adjusting the model to optimize the thermal balance. For an ideal thermal balance, the heat gain (QG) should equal the heat loss (QL). The model requires the following inputs:

Free-stream static pressure (altitude ambient), P0
Free-stream static temperature, T0
Flight Mach number, XM0
Leading-edge surface temperature, TSM
Leading-edge surface area, A
Airfoil span (inlet perimeter), S
Leading-edge thickness, D
Free-stream liquid water content (cloud), LWC
Volume median water droplet diameter, DD
Leading-edge heater power density, PA

The model outputs are:

Recovery of the water kinetic energy, QKE
Recovery of the air kinetic energy, QF
Total heat gain, QG (QKE + QF + PA)
Convective heat transfer, QC
Evaporative heat transfer, QE
Sensible heat transfer, QS
Conduction heat transfer, QK (between the leading edge and aft structural interface)
Total heat loss, QL (QC + QE + QS + QK)
Net heat transfer, QNET (QG – QL)
Calculated surface temperature, TSC

The calculated data should result in thermal balance for subsonic flight conditions provided that the input data are correct, the model is accurate, and the leading edge has reached thermal equilibrium (steady-state conditions). Two indicators were used to evaluate the degree of thermal balance achieved. The first indicator was the dependent parameter QNET, which should equal zero; i.e., the sum of the heat gain terms (QG = QKE + QF + PA) should equal the sum of the heat loss terms (QL = QC + QE + QS + QK), or QNET = QG − QL = 0.0. The second was the leading-edge surface temperature; i.e., the calculated surface temperature (TSC) should equal the measured surface temperature (TSM) when thermal balance is achieved. The calculated surface temperature was obtained by iteration of the model on the surface temperature until QNET ≈ 0.0. (In the model, iteration is complete when $|QNET| \leq 0.01$ w/in.^{2}). Since an exact thermal balance was not achieved on a data-point-by-data-point basis, the magnitude of the difference between the mean of the data set (linear curve-fit of the calculated versus measured temperatures) and the line of ideal surface temperature agreement can be used as an indicator of the extent of the thermal unbalance in terms of surface temperature, °F. The temperature difference in °F is a more comprehendible gauge of the degree of thermal balance achieved than is the unbalance in QNET in w/in.^{2}.

The available data used for the validation were obtained from AEDC tests of two similar leading-edge configurations, A and B. Both configurations are characterized by the leading-edge schematic shown in Fig. 1 where the thickness, D, was 0.22 and 0.54 in. for configurations A and B, respectively. Both configurations were equipped with electrical resistance anti-icing heaters. Only Configuration B was equipped with thermocouples for measuring the temperature gradient across the aft structural interface. The gradients were used to estimate the conduction heat loss.

Both dry- and wet-air data were acquired during the tests of both configurations, with and without the heaters in operation. The simulation of cloud icing conditions was accomplished with the icing water spray system. The water spray system was operated to produce droplets with a mass median diameter of approximately 20 μ and a uniform distribution of droplets throughout the free-jet airflow based on a prior calibration of the spray system.

The usual test procedure was to acquire steady-state dry-air test data at a constant upper airflow temperature with the heater on or off (as required to meet the test objective), activate the icing water spray system to produce inlet icing conditions (data system off), and then gradually decrease the airflow temperature 1 to 2°F/min while recording data in the transient mode. This very slow change in conditions was considered to approximate steady-state data. During one test, however, the data were acquired at steady-state conditions.

The range of flight conditions of the validation data ranged from sea level to 13,300-ft altitude, 0.45 to 0.80 flight Mach No., −6.0 to 35°F free-stream static temperature, and 0.2 to 1.5 gm/m^3 liquid water content. Leading-edge surface temperatures ranged from 10 to 80°F.

The validation was accomplished using two groups of data for both configurations, dry-air (cloud off) data and wet-air (cloud simulation) data. Because of data scatter, each group is treated as a data set, and, where appropriate, a first-order curve fit of the data set is compared to the line of ideal agreement. The estimate of the one-sigma standard deviation (SD) of the data from the curve fit is also shown.

In the first group, the effects of conduction heat loss across the aft structural interface are discussed including the procedure used to compute the conduction heat loss. The conduction heat loss relationships developed during the dry-air analysis are then used for the wet-air data analysis.

3.2 THERMAL BALANCE, CONFIGURATION A

3.2.1 Thermal Balance, Dry Air (Cloud Off)

For the dry-air case, the water-dependent terms (QE, QS, QKE) in the thermal balance equation (Fig. 1) are zero, and the equation reduces to

$$QNET = QC + QK - QF - PA$$

Initially, QK was assumed to be zero. Therefore, the equation reduces to

$$QNET = QC - QF - PA$$

The dry-air thermal balance achieved for the Configuration A test data are presented in Fig. 3, heater on and off. Ideally, if perfect thermal balance were achieved, all of the data would lie on the dashed line. Experimentally, data scatter occurred; therefore, a first-order curve fit was drawn through the data set, as shown. The maximum difference between the ideal and experimental lines was about 0.3 w/in.^{2} near the 20-w/in.^{2} level of heat loss (or gain). This is considered good agreement. Since thermal balance was essentially achieved, the initial assumption that QK = 0 was valid. The estimate of the one-sigma standard deviation of the data set (SD) from the curve-fit line was ±1.23 w/in.^{2}. The maximum deviation for a single point from the ideal agreement line was 2.0 w/in.^{2}.

The surface temperature data for the same data set are shown in Fig. 4. For the same measured temperature, the calculated surface temperature was up to 7.5°F less than the temperature required for thermal balance (corresponds to the 2 w/in.^{2} in Fig. 3). Again, a curve fit for the data set was drawn and differed from the QNET = 0.0 line (ideal agreement) by −3°F for measured surface temperatures near 50°F (corresponds to 0.3 w/in.^{2}, Fig. 3) and +1.3°F at a measured surface temperature of 10°F. This good agreement is interpreted to mean that the QC and QF terms in the thermal model are valid.

The difference between the measured and calculated leading-edge surface temperatures is presented in Fig. 5. The data spread was about 13°F. The calculated temperatures were within ±4.0°F (SD) of the measured temperatures for the data set.

3.2.2 Thermal Balance, Wet Air (Cloud Simulation)

For the wet-air case, all of the terms in the thermal balance equation are used except QK; again, QK was assumed to be zero. Therefore, the equation is

$$QNET = QC + QE + QS - QF - QKE - PA$$

The thermal balance for the wet-air data set (only heater-on data were available) are presented in Fig. 6. The data scatter was worse than the dry-air data set, and the curve fit differed from the ideal agreement line by 7.7 w/in.^{2} at the heat loss (QL) level of about 27 w/in.^{2} The difference between the calculated and measured surface temperatures corresponding to the same data set for the same 27-w/in.^{2} heat loss level was about 9.0°F (Fig. 7). The data in Fig. 6 indicate that the heat loss was too high (or the heat gain too low) and that an adjustment of the heat balance equation is required.

To adjust the model, the terms in the heat balance equation were evaluated to determine which term or terms might be adjusted to effect thermal balance of the Configuration A wet-air data set. The evaporative heat-transfer term, QE, was selected as the term for adjustment based on the following rationale. First the other terms in the equation are believed to be reasonably accurate because:

1. QC and QF were validated by the results obtained using the dry-air data,

2. QS and QKE are relatively straightforward calculations (Section 2.0), and

3. PA is a directly measured input.

Of these five terms, QF, QKE, and PA comprise the net heat gain; therefore, the net heat gain must be approximately correct. Improvement in the thermal balance, then, can be achieved only by a reduction of the net heat loss (Fig. 6). Of the candidate heat loss terms QC, QS, and QE, QC and QS are believed to be reasonably accurate for the reasons just given. This leaves QE as the choice for adjustment to improve the thermal balance. Furthermore, the mass and heat-transfer mechanisms related to the evaporative process on the leading edge are believed to be the most subject to error. Continued model development may reveal a more exacting adjustment procedure.

Continuing with the QE adjustment discussion, reduction of the net heat loss to achieve thermal balance will require a reduction in QE. This can be accomplished by multiplying QE by a fractional correlation coefficient. Application of a correlation coefficient of 0.3 (0.3 × QE) resulted in the optimum balance, i.e., positive coefficients greater than or less than 0.3 degraded the thermal balance. The results are shown in Fig. 8 where the difference between the ideal line and the data set curve-fit line is about 1.8 w/in.^{2} compared to the unadjusted difference of about 7.7 w/in.^{2} (Fig. 6). The unadjusted maximum temperature difference was 23°F (Fig. 7) compared to the adjusted maximum of −6°F shown in Fig. 9. The degree of thermal balance was less than that obtained for the dry-air data set, probably because of bias in the model. At 32°F surface temperature, the model bias was +4.5°F.

The difference between the measured and the calculated leading-edge surface temperatures for the Configuration A wet-air data are shown in Fig. 10. The data spread and the standard deviation were greater than that obtained with the dry-air data set, 18°F (compared to 13°F, Fig. 5) and ±4.8°F (compared to ±4°F, Fig. 5). Some increase in the scatter was expected because the water-dependent terms (QE, QS, and QKE) are used for the wet-air data but are zero for the dry-air case.

3.2.3 Data Summary, Configuration A

For the Configuration A dry-air test data set, the thermal model predicted the surface temperatures within about +1 to −3°F, and, for the wet-air test data set, within about +5 to −6°F, the latter after adjustment of the evaporative heat-transfer term, QE. The standard deviations of the differences between the calculated and the measured leading-edge surface temperatures were ±4 and ±4.8°F for the dry-air and the wet-air data sets, respectively. At 32°F, the model bias was +4.5°F for the wet-air data set.

Although the adjustment to QE alone did improve the data agreement, continued analysis and experimentation should result in a better understanding of all of the thermal and mass transfer processes and an improved model.

3.3 THERMAL BALANCE, CONFIGURATION B

3.3.1 Thermal Balance, Dry Air (Cloud Off)

For the Configuration B dry-air case, the water-dependent terms in the energy balance equation are zero, as before. The initial step in the analysis was to assume that QK = 0.0 and to plot the heat balance results using the Configuration B dry-air data set. These dry-air data were the only available data acquired at steady-state conditions. The results in Fig. 11 show an unbalanced condition for the heater-on data. Since the heat gain was too high by 7.5 w/in.^{2}, the unbalance was attributed to not accounting for the conduction heat loss. The conduction heat loss should be a function of the temperature differential across the aft structural interface. The available data were plotted as shown in Fig. 12, and a linear curve fit was derived from the data and used to compute the conduction heat loss, QK.

The model was rerun with the conduction heat loss calculation, and the data were replotted; the results are presented in Fig. 13. The data were within 2.0 w/in.^{2} of the ideal agreement line, and the curve fit of the data was coincident with the ideal agreement line. The corresponding calculated versus measured surface temperature data set is shown in Fig. 14; again, the data set curve-fit line was coincident with the ideal agreement line. The standard deviation for the data set curve fit was ± 1.03°F.

The differences between the measured and calculated surface temperature data for the dry-air conditions are shown in Fig. 15. This set of Configuration B data exhibited much better agreement than did the Configuration A data set. Of all the data presented in this report, this data set was the only data acquired under steady-state conditions. The standard deviation for this steady-state set was ± 1°F compared to the Configuration A dry-air data standard deviation of ± 4°F.

3.3.2 Thermal Balance, Wet Air (Cloud Simulation)

The same QK calculation derived from the dry-air data was also used for the wet-air data analysis. The wet-air data computed with this QK calculation are shown in Fig. 16. The total heat loss exceeded the total heat gain; therefore, thermal balance was not achieved. The maximum difference between the data curve-fit and the ideal agreement line was 10 w/in.^{2}. The corresponding surface temperature curve-fit for the same data set indicated a 12°F difference at a measured surface temperature of 60°F (Fig. 17).

Since a similar unbalance was experienced with the Configuration A wet-air data set, the Configuration B data were recomputed using the same 0.3 correlation coefficient for the evaporative heat loss as was used for the Configuration A data. The 10 w/in.^{2} unbalance

(Fig. 16) was reduced to 2.8 w/in.^{2} as shown in Fig. 18, a much improved degree of thermal balance. The corresponding surface temperature agreement was improved from a maximum of $-12°F$ (Fig. 17) to that shown in Fig. 19, $-3.5°F$. However, the standard deviation of the data was high ($\pm 3.04°F$). The model bias at 32°F measured surface temperature was $+3.2°F$.

The differences between the measured and calculated surface temperature data for the wet-air conditions are presented in Fig. 20. These Configuration B data exhibited a similar range of temperature differences with about a $\pm 1°F$ improvement in the standard deviation compared to the Configuration A wet-air data set (Fig. 10).

3.3.3 Data Summary, Configuration B

After accounting for aft structural interface conduction heat loss, excellent agreement was obtained between the calculated and measured surface temperatures for the dry-air data set. For the wet-air data set computed with the model adjustment, the calculated-to-measured surface temperature curve-fit line was a maximum of 3.5°F below the ideal agreement line, but the standard deviation of the set was high (3.04°F). The standard deviations of the differences between the calculated and measured leading-edge surface temperatures were ± 1 and $\pm 4°F$ for the dry-air and wet-air data sets, respectively. For the wet-air data set, the model bias was $+3.2°F$ at 32°F measured surface temperature.

3.4 DATA UNCERTAINTY

The uncertainties of the measured test data used as input parameters to the model were propagated through the model to obtain an estimated uncertainty of the primary calculated parameters, heat loss, QL, and heat gain, QG. The sensitivities (influence coefficients) for the model discussed in Section 4.1 of this report were combined with the bias and precision of the measured data using the procedure described in Ref. 11. The results for a nominal flight condition are shown in Table 1. The uncertainty of the model is not known but is probably no better than the 5- to 9-percent uncertainties shown in Table 1. Therefore, the total uncertainty of the calculated data obtained from the measured inputs and the model is probably on the order of 15 to 20 percent.

3.5 SUMMARY

Using the available AEDC test data, the degree of thermal balance achieved and the corresponding correlation of the calculated and measured leading-edge surface temperatures were used to validate the thermal model. An evaporative heat loss correlation coefficient,

EC, of 0.3 was used to optimize the agreement between the calculated and measured surface temperatures. The resultant heat balance equation thus becomes

$$QNET = HC(TS - TO) + (EC)\,(MPR)\,(M/A)L + (M/A)CW(TS - TO) + QK - HC(R)V^2/2GJ(CA) - (M/A)V^2/2GJ - PA$$

where

$$EC = 0.3$$

Using this coefficient, the model is considered validated to the extent possible with the two groups of available data. At 32°F surface temperature, the average model bias is about 4°F. Continued thermal model development should improve the model accuracy.

4.0 MODEL OUTPUT PARAMETER CHARACTERISTICS

The validated model (with the 0.3 evaporative correlation coefficient) was operated at typical incipient icing conditions with the input parameters varied to determine the corresponding effects on the output or calculated parameters. The results are presented to assist the reader in evaluating the relative effects. The aft interface conduction heat loss term, QK, was omitted to simulate an adiabatic leading-edge structural interface (Fig. 1).

4.1 MODEL SENSITIVITY

Each input parameter was varied +1 percent from the typical flight condition of Mach No. 0.55, 3,000-ft altitude, where the altitude ambient static pressure, P0, was based on Ref. 12. The altitude ambient static temperature was chosen such that thermal balance is achieved (i.e., QNET = 0.0) and is a temperature conducive to icing. All of the input conditions chosen for this typical flight condition are shown in the third vertical column in Table 2 and are designated the base conditions. Without the 1-percent perturbation, the values of the base output parameters are shown for reference on the second line of the table. The remainder of the table lists the percent changes in each output parameter for a 1-percent increase in each input parameter. The +1-percent change data are presented in Fig. 21 to show the relative effects on the output parameters, which generally varied from −1.0 to +1.0 percent. However, a 1-percent increase in TS resulted in a 1.86-percent increase in the evaporative heat transfer (QE). A 1-percent increase in XM0 resulted in a 2.5-percent increase in QF and a 3.1-percent increase in QKE.

The changes in QNET in w/in.^{2} are shown in Fig. 22. QNET is sensitive to XM0 but is most sensitive to TS. Therefore, when preparing the criteria for a test or experiment, accurate measurement of these parameters is essential.

4.2 HEAT LOSS AUDIT

The relative contribution of each of the heat loss terms (QC, QE, QS) to the total heat loss (QL) was calculated as the percent of the total heat loss and is presented in Fig. 23 as a function of liquid water content (LWC) for one flight condition. At zero LWC, all of the heat loss is convective (100 percent). As LWC is increased, QC decreases and QE increases up to LWC = 0.0165 gm/m^3. For these lower portions of the QC and QE curves (LWC $\leq$ 0.0165), all of the intercepted water is being evaporated, i.e., MPR = 1.0. Above LWC = 0.0165 as LWC is further increased, the percentage of water evaporated progressively decreases (MPR < 1.0)—the remainder being runback. The convective heat transfer, QC, and the evaporative heat transfer, QE, decrease as the percentage of sensible heat transfer, QS, progressively increases with increasing LWC.

The calculated QC and QE data exhibited approximately 16 percentage point changes between LWC values of zero and 0.0165 gm/m^3. This vividly indicates that the maximum evaporative cooling, percentage-wise, occurs at low values of LWC.

5.0 MODEL APPLICATIONS

The model may be used to analyze the thermal energy balance on the leading edge of small airfoils. To date, application of this model has been limited to leading-edge thickness (D) values near 0.5 in., volume (or mass) median droplet diameters (DD) from 10 to 30 microns, altitudes below 15,000 ft, flight Mach numbers (XM0) up to 0.8, free-stream static temperatures (T0) from −25 to 32°F, leading-edge surface temperatures (TS) from 32°F (instantaneously) to 130°F (continuously), and liquid water contents (LWC) up to 3.0 gm/m^3.

The model uses an estimate of the boundary-layer temperature (TF) as suggested in Refs. 4 and 13 which is the average of the free-stream static temperature and the surface temperature for the calculation of transport properties (e.g., HC) and the associated air properties (MU, K, RHO). Measurement of the actual boundary-layer properties should improve the accuracy of the calculated results.

The accuracy of the modified inertia parameter is quoted as ±5 percent in Ref. 6. Accuracy may be improved by using a more rigorous water droplet trajectory analysis. This requires an accurate description of the flow field about the leading edge which can be obtained from experimental measurements or estimated using computational fluid dynamics. If the leading edge being evaluated is in close proximity to other aerodynamic surfaces (e.g., the airframe forebody, control surfaces, etc.), the effects of the changes in flow field from ideal free-stream conditions should be accounted for in the model inputs.

Icing tests of airframe systems have become more common in recent years in wind-tunnel-type ground test facilities because of improved capabilities for producing, controlling, and measuring icing environmental conditions. However, because of recent escalations in energy costs, wind tunnel test time has become increasingly expensive. Test time can be minimized by predicting the effects of LWC on the test article surface temperature for a given free-stream static temperature or vice versa. In addition measured data can be input to the model and the results used to analyze and evaluate the measured parameters. Examples of model applications are presented in the remainder of this section for an airfoil leading-edge thickness of 0.045 ft. The validated model was used for the calculations.

5.1 EFFECTS OF VARYING LIQUID WATER CONTENT

5.1.1 Surface Recovery Temperature

One application of the model is to determine the average equilibrium surface temperature (or recovery temperature) of the leading edge for a given set of environmental conditions. As an example, the surface temperature was calculated as a function of LWC for two flight Mach numbers at 3,000-ft altitude. Setting T0 = 30°F and QK and PA = 0.0, the model was iterated on TS until QNET ≈ 0.0 (|QNET| ≤ 0.01 w/in.^{2}, TS within ±0.05°F). The results for flight Mach numbers 0.4 and 0.8 are plotted in Fig. 24a. At 0.4 Mach number, the average surface temperature decreased from 43.5°F, the dry recovery temperature, to 40.5°F as LWC increased from 0.0 to about 0.013 gm/m^3 or a rate of change of 230°F/gm/m^3. Further increase in LWC up to 3.0 gm/m^3 reduced the surface temperature to 36.5°F, only an additional 4.0°F. Over the full range of LWC change from 0.0 to 3.0 gm/m^3, the total change in surface temperature was only 7.0°F. Therefore, at 0.4 Mach number, TS is relatively insensitive to LWC. At 0.8 Mach number, however, the initial rate of change was higher (304°F/gm/m^3), but the total change for the same change in LWC was 28.4°F. As noted previously, the inflection points occur at the transition of MPR from a value of unity to a value less than unity or where runback initiates as LWC is increased.

A typical range of test LWC's is 0.1 to 1.5 gm/m^3. For this range, the change in surface temperatures at flight Mach numbers 0.4 and 0.8 were 2.3 and 8.5°F, respectively (Fig. 24a). Since this 15:1 change in LWC produced relatively small changes in surface temperature, LWC settings in this range are not critical for incipient icing tests.

The effects of flight Mach number and altitude on surface temperature were investigated at a constant LWC = 1.5 gm/m^3. At 3,000-ft altitude, the surface temperatures were 37.7 and 57.3°F for 0.4 and 0.8 Mach numbers, respectively, or a difference of 19.6°F (Fig. 24a). Referring to Fig. 24b for 0.4 Mach number, the calculated surface temperatures at 3,000-and 15,000-ft altitudes (LWC = 1.5 gm/m^3) were 37.8 and 36.9°F, respectively, a difference of only about 1.0°F. Therefore, surface temperature is affected more by flight Mach number than by altitude.

5.1.2 Free-Stream Static Temperature

Another application of the model is to evaluate the relative change in free-stream static temperature, T0, with LWC. The procedure used was to set TS = 34°F, QK and PA = 0.0, and to iterate the model on T0 until QNET $\approx$ 0.0 (absolute value of QNET $\leq$ 0.01 w/in.^{2}, as before) while increasing LWC from 0.0 to 3.0 gm/m^3 at 3,000-ft altitude. The effect of changing flight Mach number from 0.4 to 0.8 was also calculated, and the results are presented in Fig. 25a. The total change in T0 for an increase in LWC from 0.0 to 3.0 gm/m^3 was 6.6 and 25.7°F, respectively, for flight Mach numbers of 0.4 and 0.8.

The effect of changing altitude is shown similarly in Fig. 25b. Again, the effect of altitude is relatively small for the 0.0 to 3.0 gm/m^3 change in LWC. The changes were 6.5 and 7.2°F at altitudes of 3,000 and 15,000 ft, respectively.

5.2 ICING ONSET PREDICTIONS

Data generated by iteration of the model on T0 can be used to provide predictions of icing onset for a 32°F surface temperature. A primary test objective of one of the two test configurations discussed previously was to determine the inlet leading-edge icing onset temperatures. The thermal model was used to predict icing onset for a range of flight conditions prior to acquisition of the test data used for model validation. The free-stream and local flow properties were assumed identical, as in the case of an isolated airfoil, one where the flow field is unaffected by proximate bodies. The pretest predictions for a 32°F surface temperature are shown in Fig. 26 for three altitudes and liquid water contents.

A comparison of the predictions and test results is shown in Fig. 27. The upper and lower boundaries identified in Fig. 26 are replotted in Fig. 27 as dashed lines. The test results are represented by the cross-hatched band. The isolated airfoil predictions agreed with the test results within 1 to 4°F only at a flight Mach number of 0.6. At Mach number 0.5, icing occured at free-stream static temperatures about 5°F higher than predicted. Above Mach number 0.6, the predicted temperatures were higher than the test results, up to about 14°F at Mach number 0.8. The effect of using the 0.3 evaporative correlation coefficient (the validated model) is shown by the solid-line boundaries. This improved the agreement at the higher Mach numbers but degraded the agreement at the lower flight speeds. A more extensive survey of the local flow conditions should improve the results, but further model development is also needed to improve the icing onset predictions.

5.3 ANTI-ICING HEATER SIZING

The model can also be used for determing the leading-edge heater capacity. Two such applications are discussed below.

5.3.1 Reducing Icing Onset Temperature

Referring to Fig. 26, the family of curves can be shifted to the left by applying internally generated heat to the leading edge using, for example, a heating device, PA, as shown schematically in Fig. 1. To illustrate the effect of heat addition, the iterative solution for the icing onset boundary for TS = 32°F, 3,000-ft altitude, and LWC = 0.5 gm/m^3 is shown in Fig. 28 (QK = 0.0). The curve was shifted to the left by incrementally setting PA at 5 and 10 w/in.^{2}, decreasing the free-stream static temperature at which icing onset would occur at 0.5 flight Mach number by 18.6 and 38.5°F, respectively. This technique can be used along with the flight system mission objective to improve the margins for ice-free operation, i.e., to enlarge the ice-free flight envelope.

5.3.2 Dry Anti-Icing

For some flight systems, it may be desired to size a heater for complete evaporative anti-icing, referred to by Sogin (Ref. 9) as dry anti-icing. To satisfy this requirement, TS must be increased until MPR = 1.0, i.e., until all of the intercepted water is evaporated (zero runback). Application of the validated model for dry anti-icing is illustrated in Fig. 29 for three liquid water contents at the 0.4 Mach number, 3000-ft altitude, 20°F T0 flight condition. The power density required is 8.9, 32.7, and 58.6 w/in.^{2}, respectively, for liquid water contents of 0.1, 0.5, and 1.0 gm/m^3. The dry anti-icing power density was obtained by increasing TS until MPR = 1.0. The corresponding surface temperatures required for dry anti-icing are 67.2, 114.0, and 138.3°F.

5.4 TEST DATA ANALYSIS

The thermal model can also be used to analyze and evaluate the leading-edge thermal balance data obtained from wind tunnel test and/or flight test. Careful attention should be given to the uncertainty of the measured inputs XM0, P0, LWC, DD, TS, D, A, QK, and PA. Some insight on this subject can be obtained from the sensitivity study presented in Section 4.1 of this report. LWC and DD require calibration of the wind tunnel water spray system or measurement during the flight test. The leading-edge thickness, D, and surface area, A, require the measurement of physical dimensions which are more difficult for small-thickness airfoils. If the leading-edge contour is not strictly a half-cylinder, then the surface area should be measured and converted to an equivalent cylindrical diameter (using measurement of the span), or the more appropriate E versus K0 relationship for the particular leading-edge shape should be used.

For test data analysis, the model should be calibrated or verified. The ideal procedure would be to check each term of the heat balance equation individually. Since the terms are interactive, however, the terms can only be checked in groups. This can be done progressively in three steps. By inputting the measured parameters for a dry-air calibration test (Step 1), the terms QC and QF can be evaluated quantitatively as a group. Similarly, during a wet-air calibration test (Step 2), the effect of the terms which are functions of LWC (QE, QS, and QKE) plus QC and QF, all five terms, can be investigated as a group. And finally, with the heater on (Step 3), the computed results for the complete equation should result in thermal balance.

Steps 1 and 2 require that no (or negligible) thermal gradients exist across the structural interface. This must be confirmed by measurement. For Step 3, measurement of the gradient is also required since a temperature difference across the interface will probably exist with the heater on.

Step 3 requires an input for QK. Quantitative calculation of QK is usually difficult because the structural complexity of the interface configuration complicates the determination of the effective conduction heat-transfer coefficient and because materials are often used for which the coefficient is unknown. However, QK can be estimated using the following procedure. First (Step A), measure the temperature gradient (ΔT) across the structural interface while flowing dry air. With QNET set equal to zero (also QE, QS, and QKE = 0.0 for dry air) and the heater off, then QK equals 0.0 (provided, of course, that $\Delta T \approx 0.0$) and QC equals QF. Secondly (Step B), repeat Step A with the heater on at constant power, again measuring ΔT. Assuming that QF still equals QC, then the following cancellation applies:

$$QK = \cancel{QF} + PA - \cancel{QC} = (K/X)\,\Delta T$$

Therefore, the conduction heat-transfer coefficient, K, equals (PA)X/ΔT. Step B should be repeated for each anticipated heater power setting.

Steps 3 and B also require an input for PA. The most convenient arrangement for determining the power density is the use of an electrical heater for which the electrical power consumption is measured directly. Heater end fittings or other extraneous sources of heat loss require close scrutiny.

Model verification Steps 1 through 3 should be accomplished for each planned flight condition.

Once the above steps have been completed, one can evaluate the thermal characteristics of the leading-edge system by inputting the measured parameters and plotting QG versus QL. Ideally, the data should fall on a line connecting all points where QG = QL or QNET = 0.0. In reality, QNET ≠ 0.0. Some assessment of the TS data quality can be made by omitting TS as an input (since the model is most sensitive to TS), iterating the model on TS until QNET ≈ 0.0, and evaluating the differences between TS calculated and TS measured.

6.0 SUMMARY OF RESULTS

1. A relatively simple steady-state thermal model has been developed to assist in predicting incipient icing on wings, fins, and inlet leading edges of small subsonic missiles and drones.

2. The model is primarily a heat balance of the component leading edge and treats the effects of free-stream Mach number, altitude, cloud liquid water content, and vehicle anti-ice heaters.

3. The model has proved to be useful in predicting the effects of liquid water content on vehicle surface temperature, hence the onset of icing, during free-jet wind tunnel tests. This capability has reduced the required test time, thus reducing energy costs and total test costs.

4. The model is useful for related applications, e.g.,

   a. Determining the free-stream static temperature for a specified surface temperature with varying liquid water content

b. Sizing anti-icing heaters

c. Analyzing wind tunnel or flight test incipient icing test data.

5. Analytical application of the steady-state model has been limited to the following conditions:

   a. Leading-edge thickness, 0.22 to 0.54 in.

   b. Volume median droplet diameters, 10 to 30 μ

   c. Altitudes up to 15,000 ft

   d. Mach numbers up to 0.8

   e. Free-stream static temperatures, -25 to 32°F

   f. Leading-edge surface temperatures, 32 to 130°F

   g. Liquid water contents up to 3.0 gm/m^3.

6. Using the available AEDC test data, correlations of the calculated and measured leading-edge surface temperatures were used to validate the thermal model. The average model bias is about $+4$°F at a surface temperature of 32°F.

REFERENCES

1. Messinger, Bernard L. "Equilibrium Temperature of an Unheated Icing Surface as a Function of Air Speed." Presented at the Design and Structures Session, Annual Summer Meeting, I.A.S., Los Angeles, California, June 27-28, 1951.

2. Willbanks, C.E. and Schulz, R. J. "Analytical Study of Icing Simulation for Turbine Engines in Altitude Test Cells." AEDC-TR-73-144 (AD770069), November 1973.

3. Kreith, Frank. *Principles of Heat Transfer*. International Textbook Company, Scranton, Pennsylvannia, 1958.

4. Bowden, D. T., et al. "Engineering Summary of Airframe Icing Technical Data." FAA-ADS-4 (AD608865), March 1964.

5. *U.S. Standard Atmosphere, 1976.* U.S. Government Printing Office, Washington, D.C., October 1976.

6. *Aerospace Applied Thermodynamics Manual.* Society of Automotive Engineers, October 1969 (Second Edition).

7. Keenan, J. H. and Keyes, F. G. *Thermodynamic Properties of Steam.* John Wiley & Sons, Inc., New York, 1947.

8. Dorsey, N. Ernest, ed. *Properties of Ordinary Water-Substance in All Its Phases.* American Chemical Society Monograph Series, Reinhold Publishing Corporation, New York, 1940.

9. Sogin, Harold H. "A Design Manual for Thermal Anti-Icing System." WADC-TR-54-313, December 1954.

10. *ASHRAE Handbook of Fundamentals.* American Society of Heating, Refrigerating and Air-Conditioning Engineers, Inc., New York, 1974.

11. Abernethy, R. B., Thompson, J. W., Jr., et al. "Handbook Uncertainty in Gas Turbine Measurements." AEDC-TR-73-5 (AD755356), February 1973.

12. *U.S. Standard Atmosphere, 1962.* U. S. Government Printing Office, Washington, D.C., December 1962.

13. Eckert, E. R. G. and Drake, R. M. *Heat and Mass Transfer.* McGraw-Hill Book Company, Inc., New York, 1959 (Second Edition).

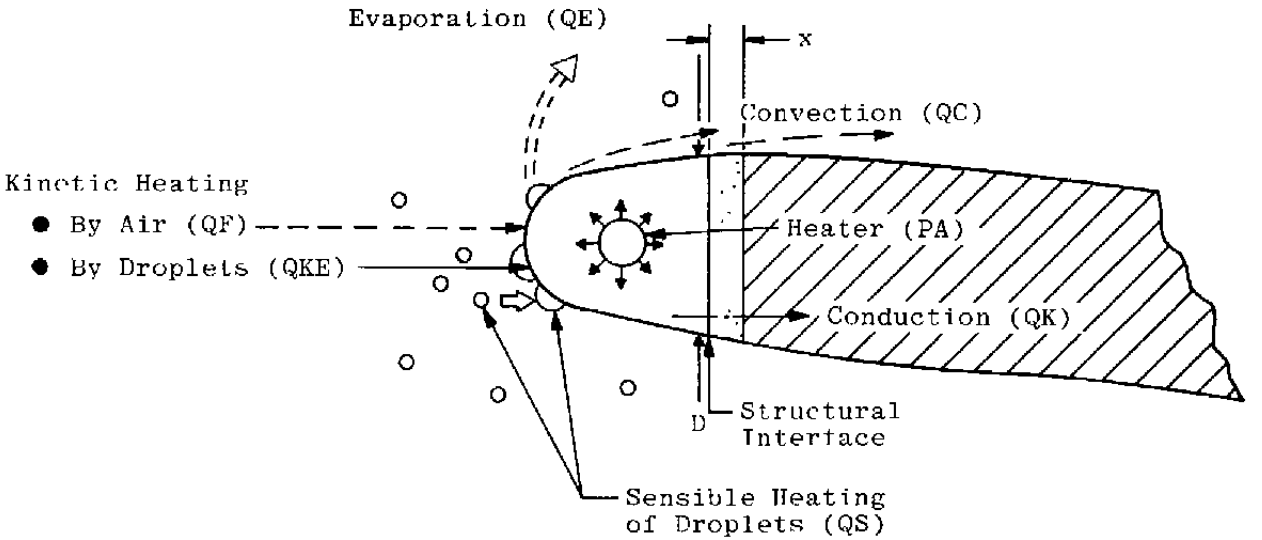

Steady-State Heat Balance Equation

$$QNET = \underbrace{QC}_{\text{Convective}} + \underbrace{HC(TS - TO)}_{\text{Convective}} + \underbrace{(EC)^{*}\ MPR\ (M/A)L}_{\text{Evaporative}} + \underbrace{QE}_{\text{Evaporative}} + \underbrace{(M/A)\ CW\ (TS - TO)}_{\text{Sensible}} + \underbrace{QS}_{\text{Sensible}} + \underbrace{QK}_{\text{Conduction}}$$

Heat Loss Terms

$$- \underbrace{HC(R)\ V^2/2GJ(CA)}_{\text{Air}} - \underbrace{QF}_{\text{Air}} - \underbrace{(M/A)\ V^2/2GJ}_{\text{Water}} - \underbrace{QKE}_{\text{Water}} - \underbrace{PA}_{\text{Heater}}$$

Heat Gain Terms

Kinetic Energy

*EC, Evaporative Correlation Coefficient (Added During Model Validation)

Figure 1. Typical leading-edge system and heat balance equation.

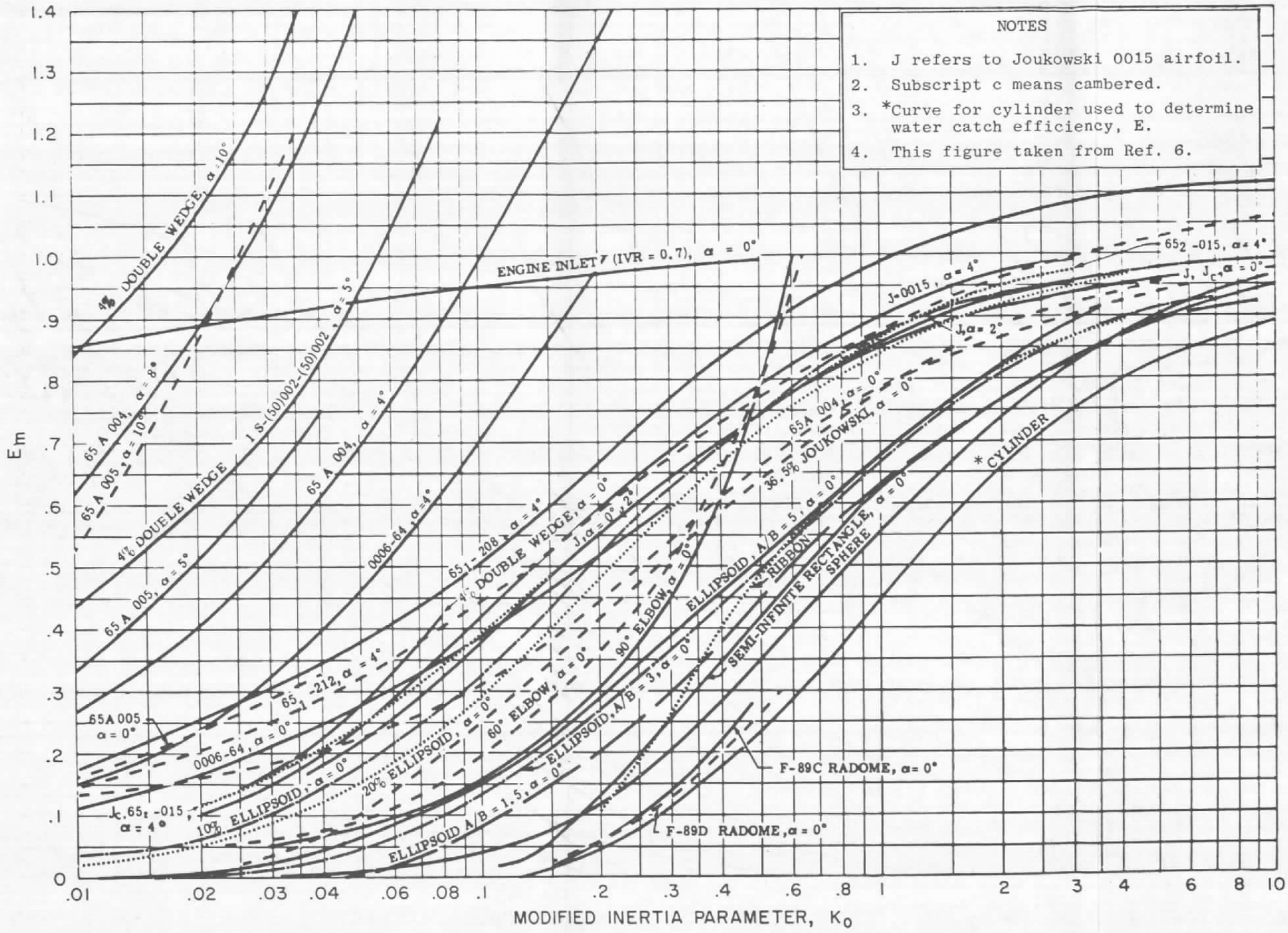

Figure 2. Water catch efficiencies.

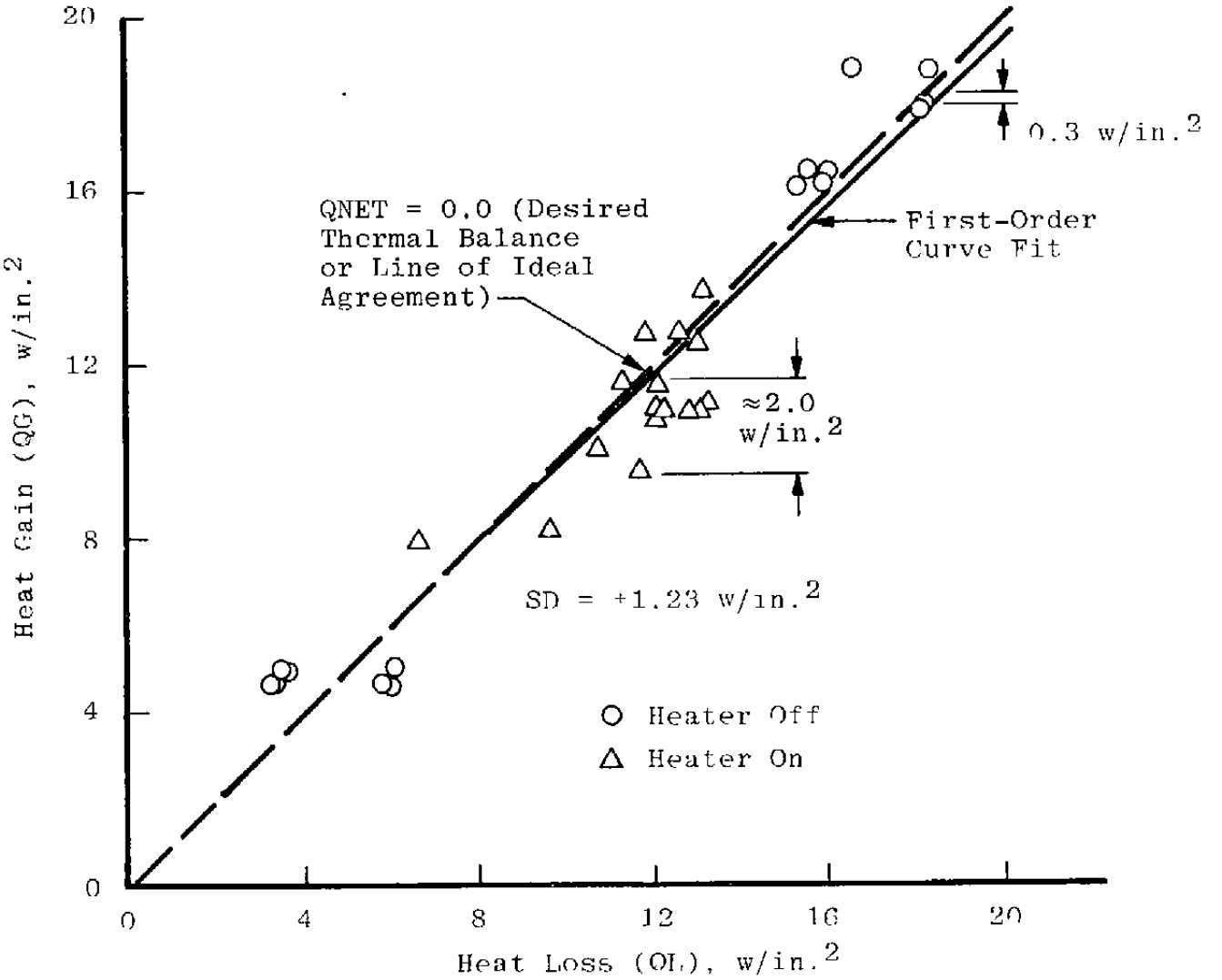

Figure 3. Thermal balance, dry air (Configuration A).

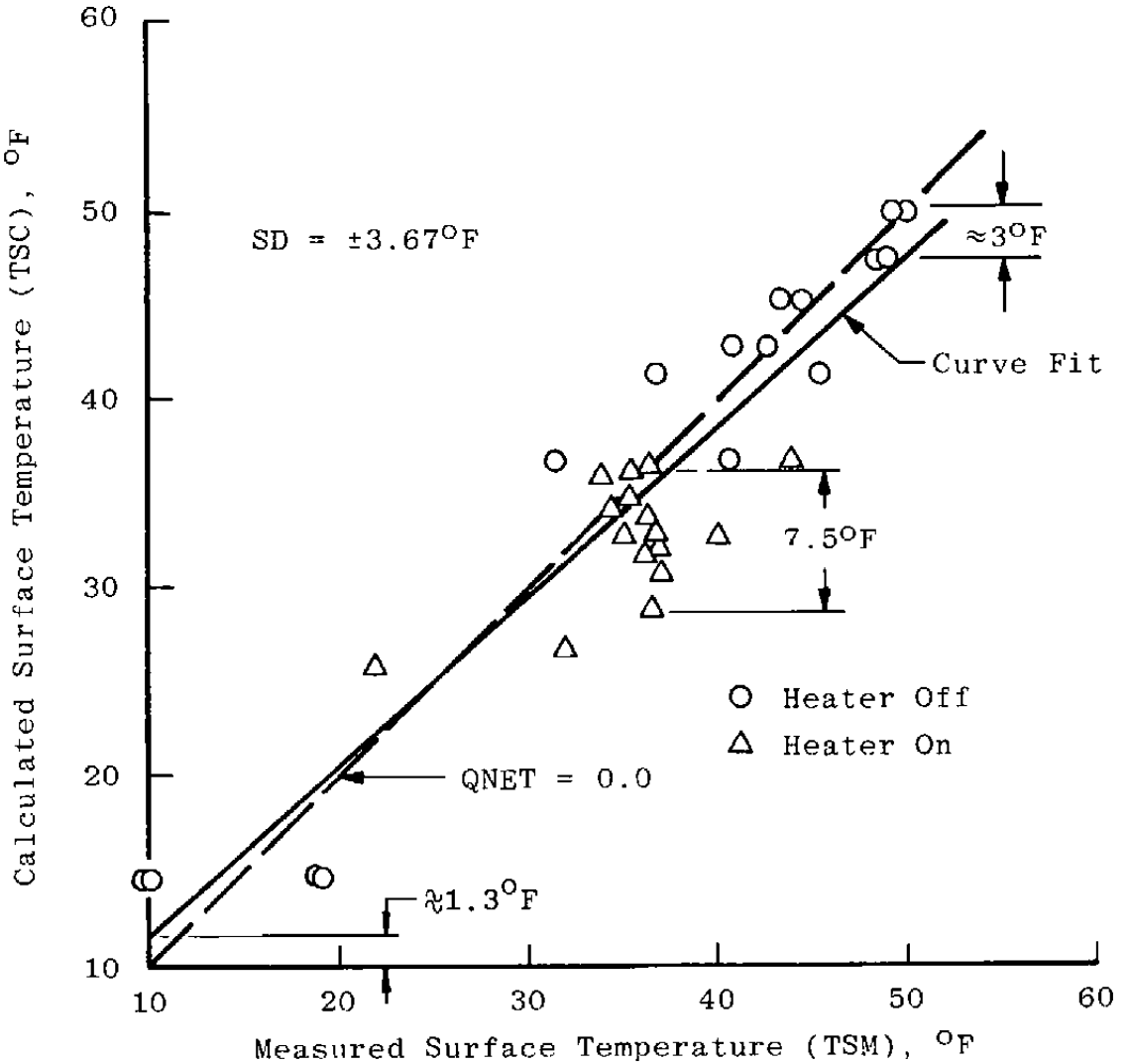

Figure 4. Calculated versus measured surface temperature, dry air (Configuration A).

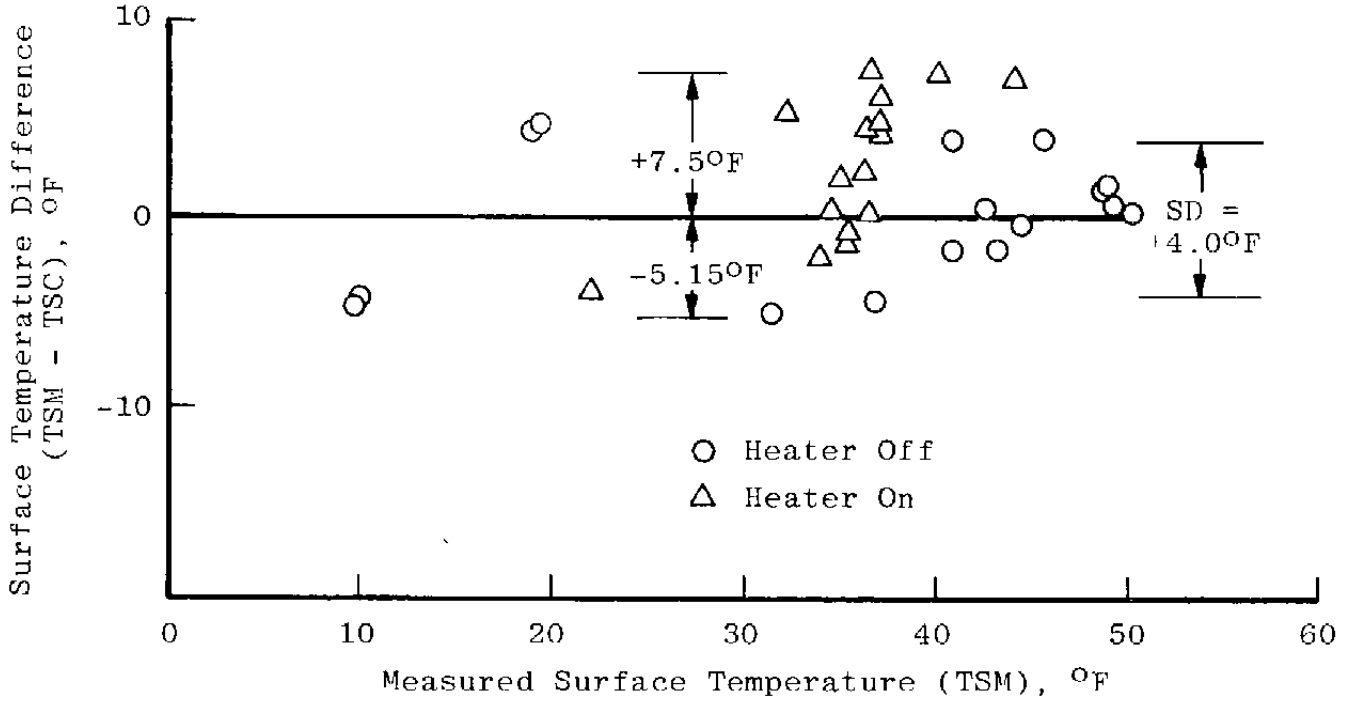

Figure 5. Difference between measured and calculated leading-edge surface temperatures, dry air (Configuration A).

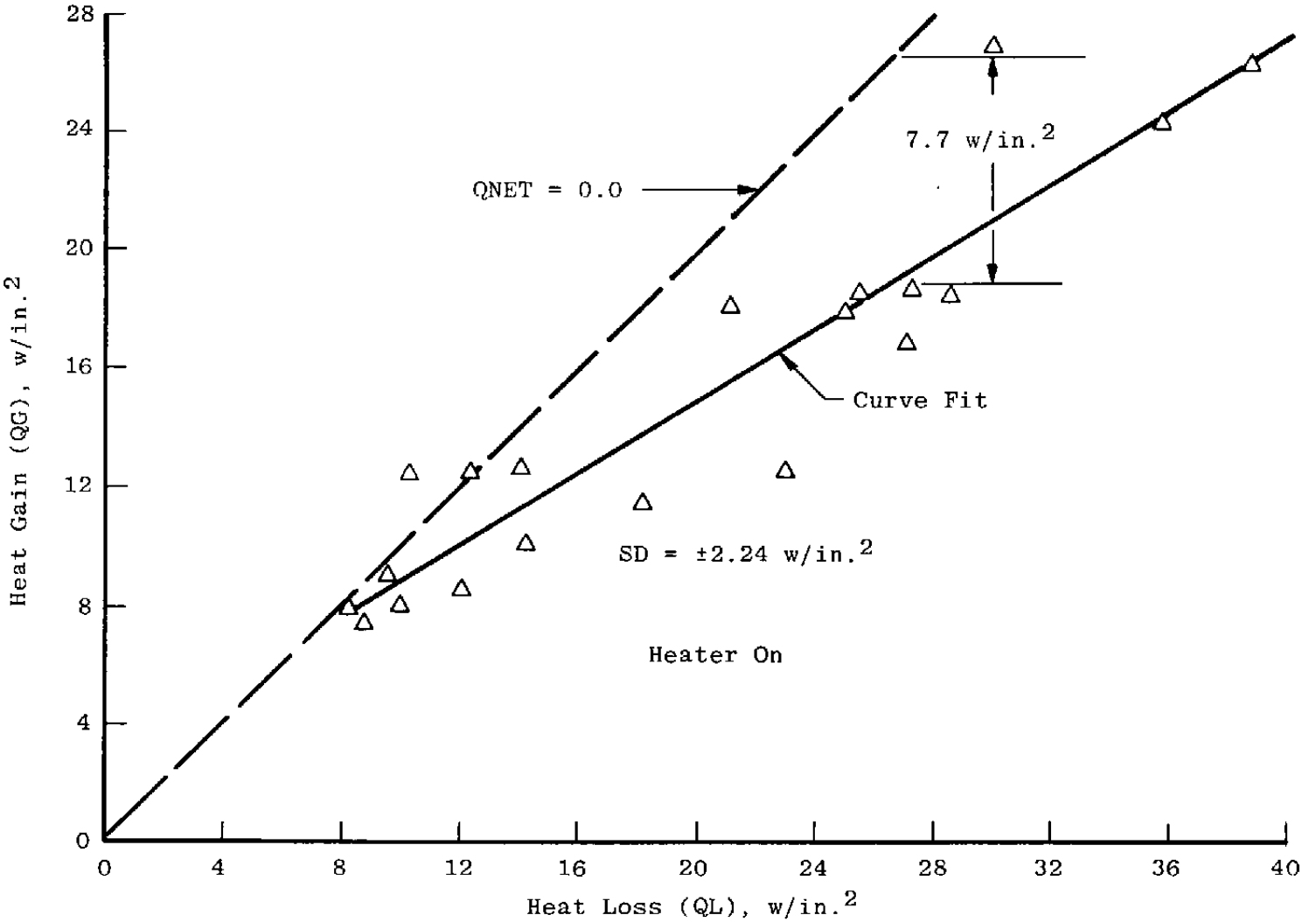

Figure 6. Thermal balance, wet air (Configuration A).

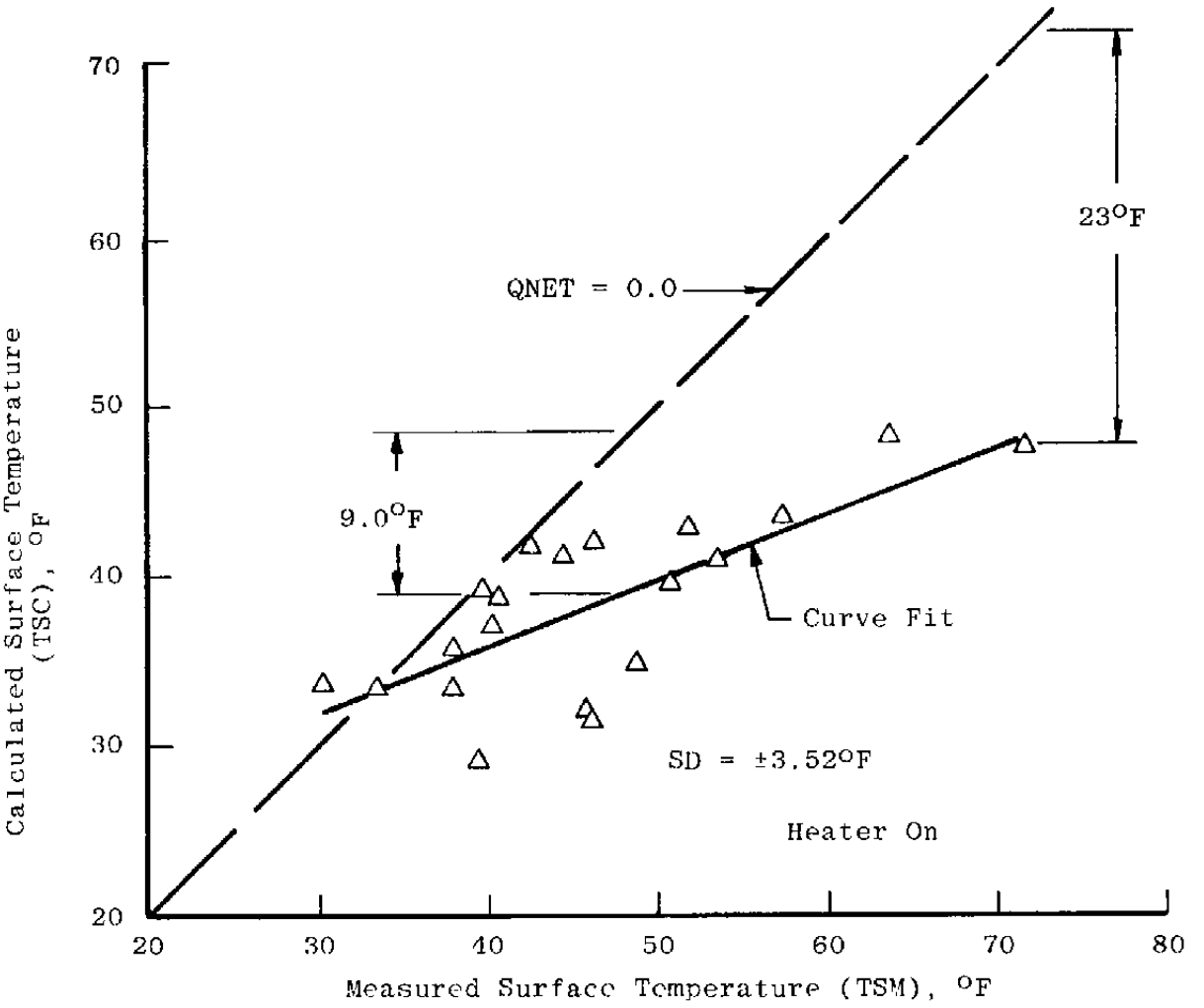

Figure 7. Calculated versus measured surface temperature, wet air (Configuration A).

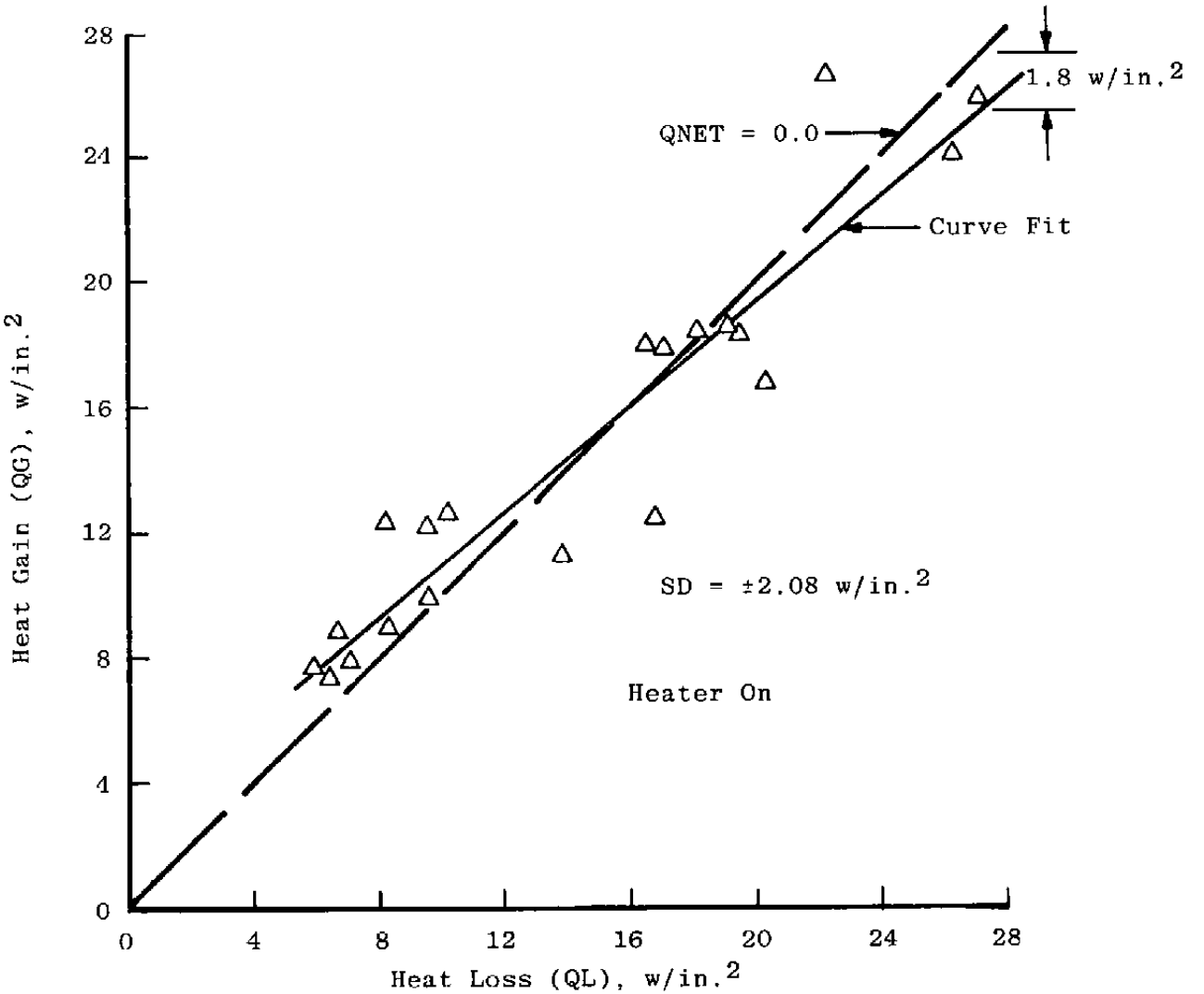

Figure 8. Thermal balance, model adjusted, wet air (Configuration A).

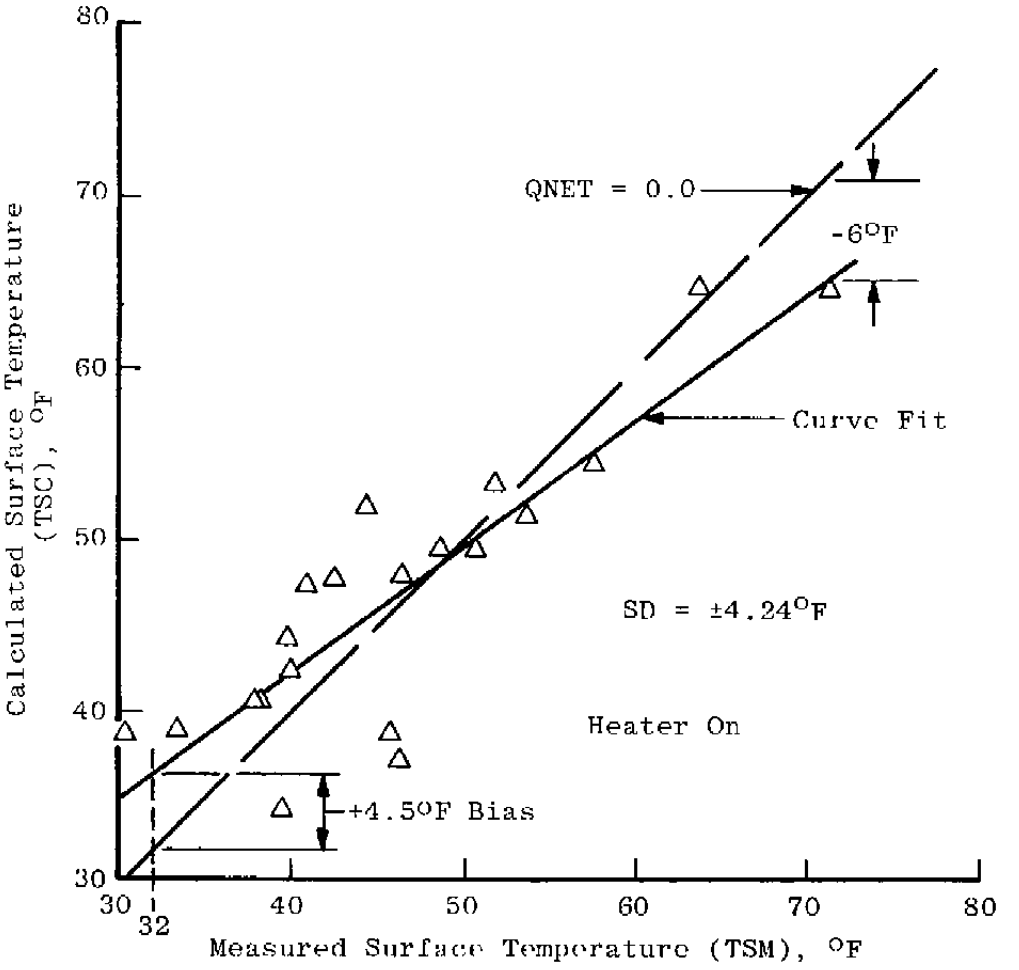

Figure 9. Calculated versus measured surface temperature, model adjusted, wet air (Configuration A).

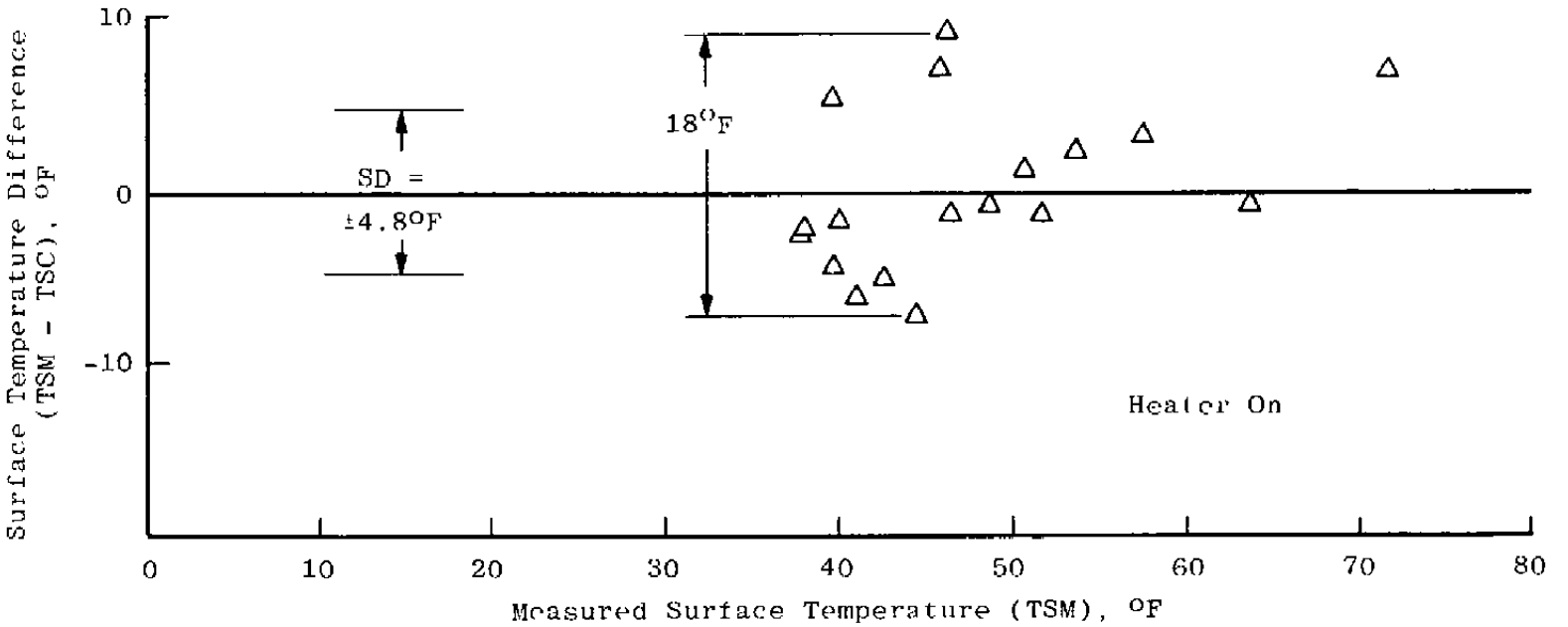

Figure 10. Difference between measured and calculated leading-edge surface temperatures, model adjusted, wet air (Configuration A).

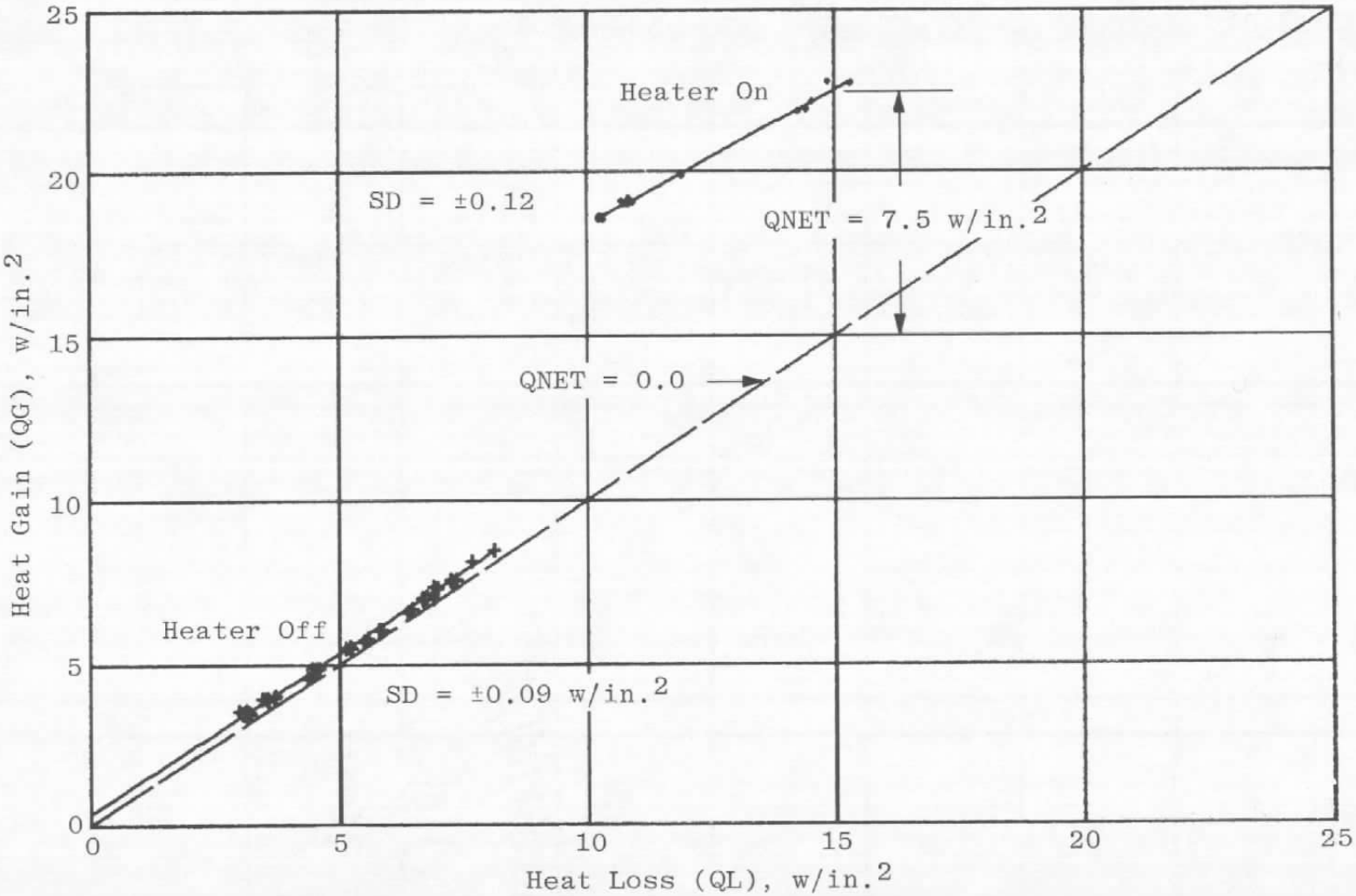

Figure 11. Thermal balance, dry air, QK = 0.0 (Configuration B).

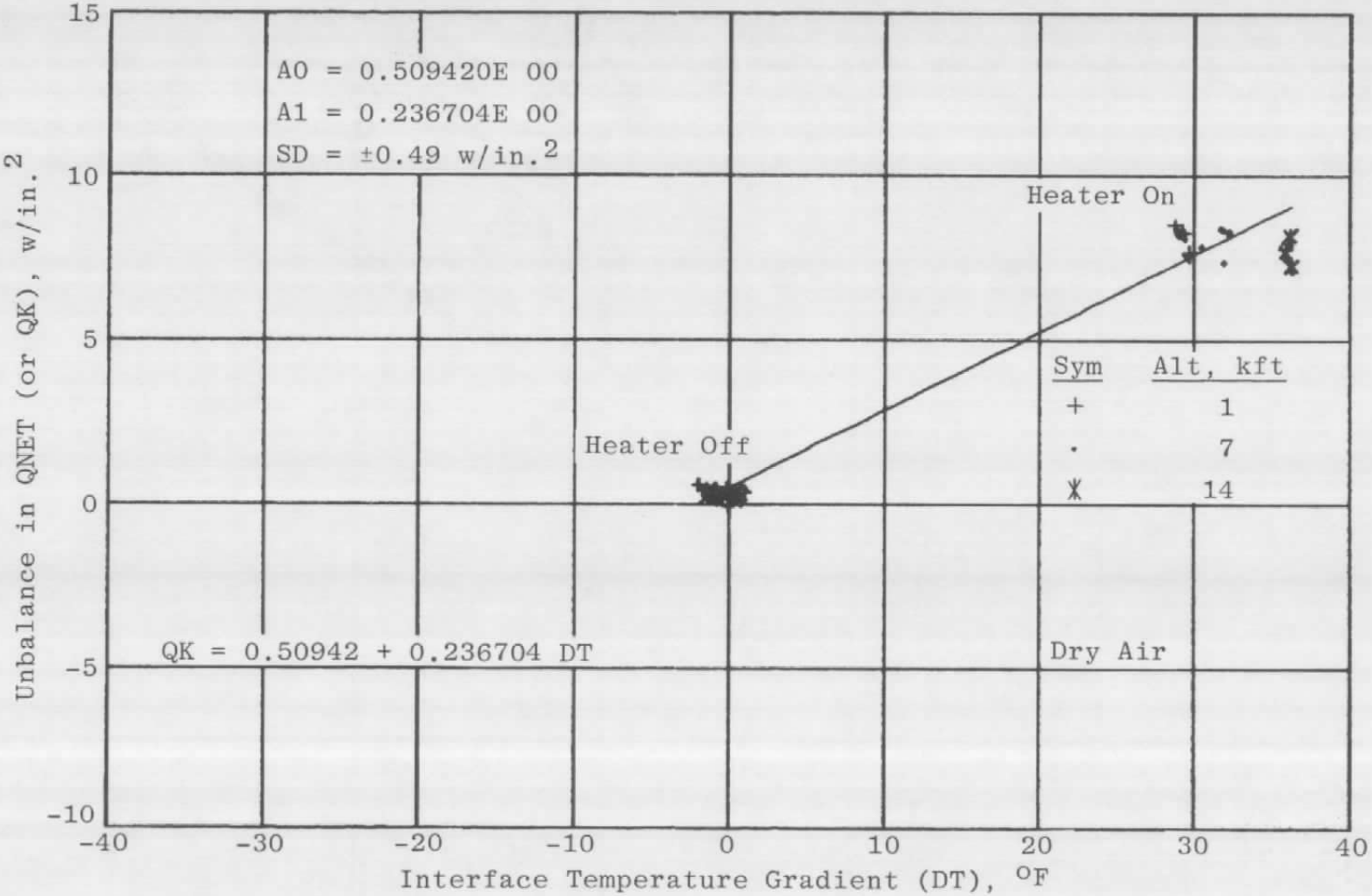

Figure 12. Conduction heat loss as a function of structural interface temperature gradient (Configuration B).

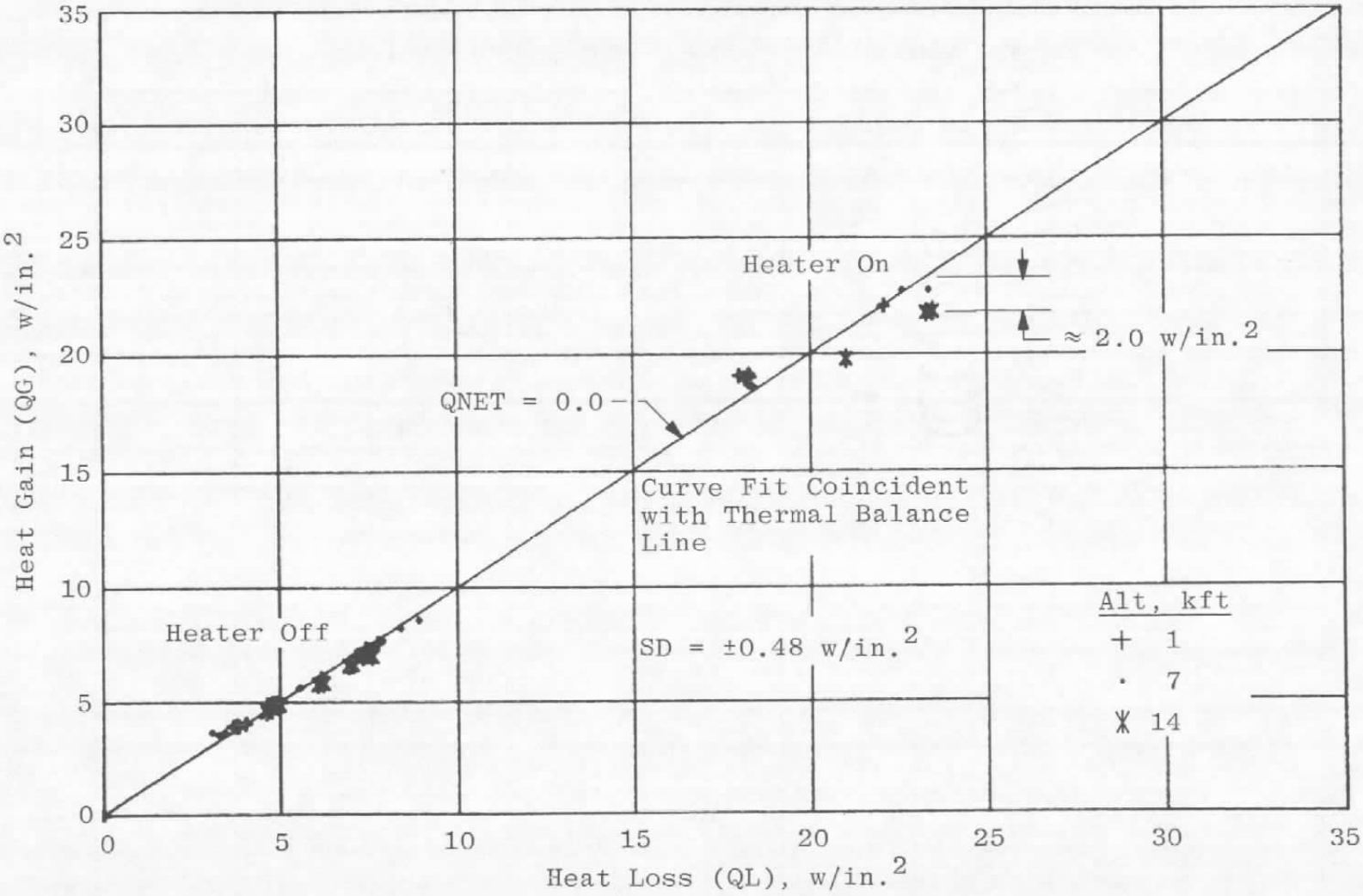

Figure 13. Thermal balance, dry air, QK = f (DT) (Configuration B).

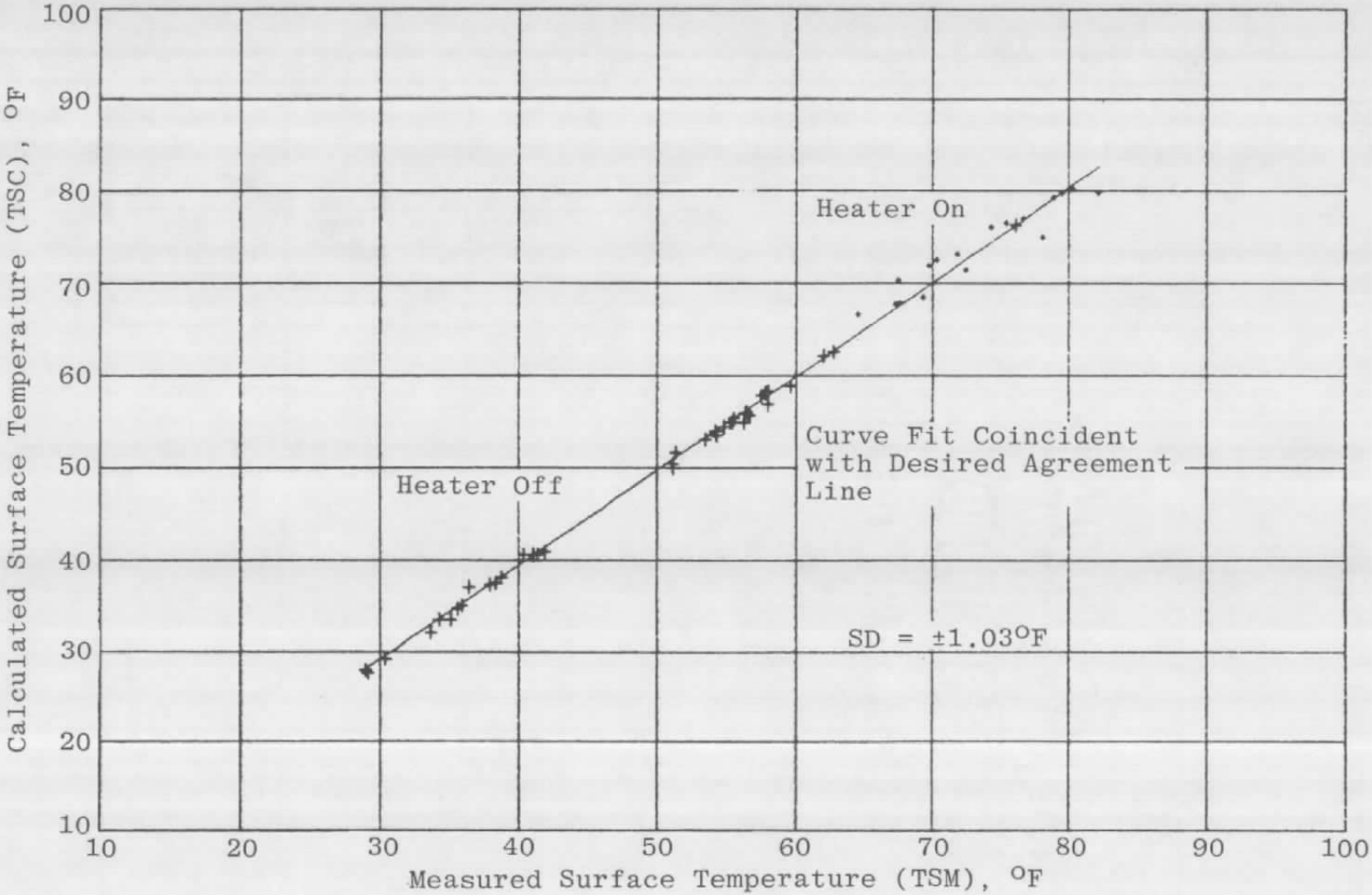

Figure 14. Calculated versus measured surface temperature, dry air (Configuration B).

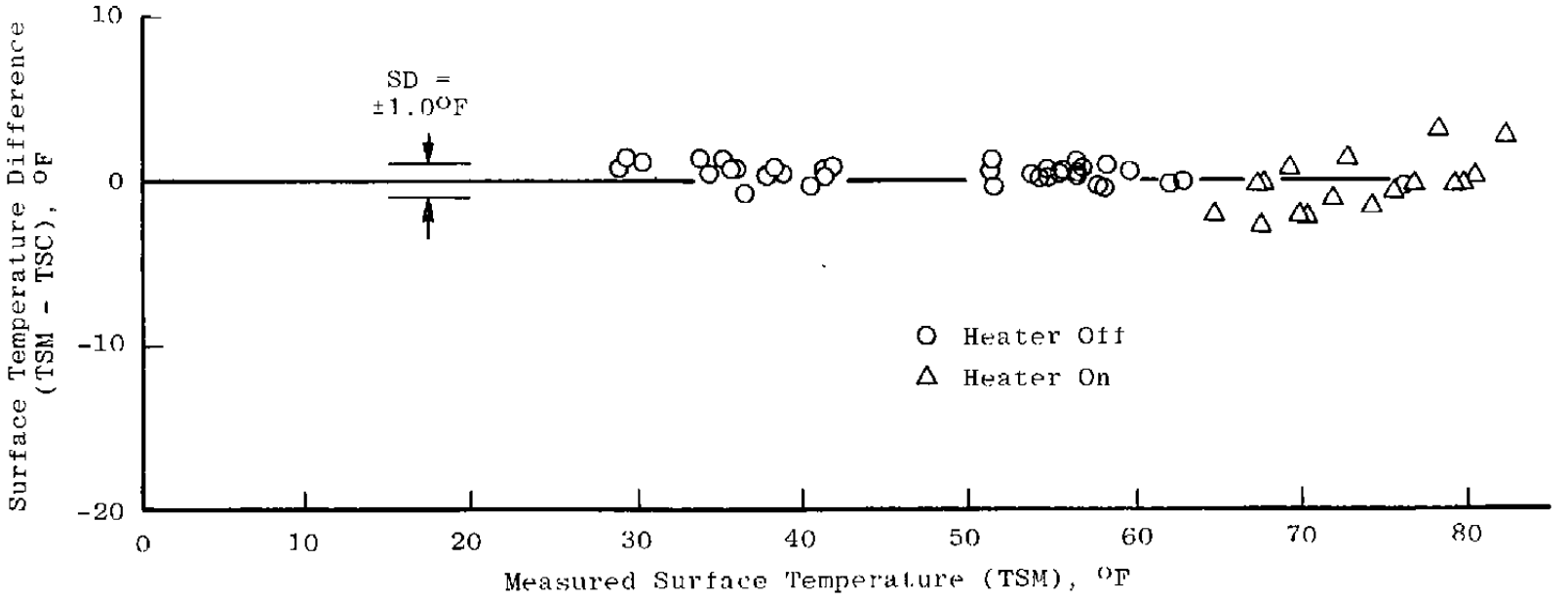

Figure 15. Difference between measured and calculated leading-edge surface temperatures, dry air (Configuration B).

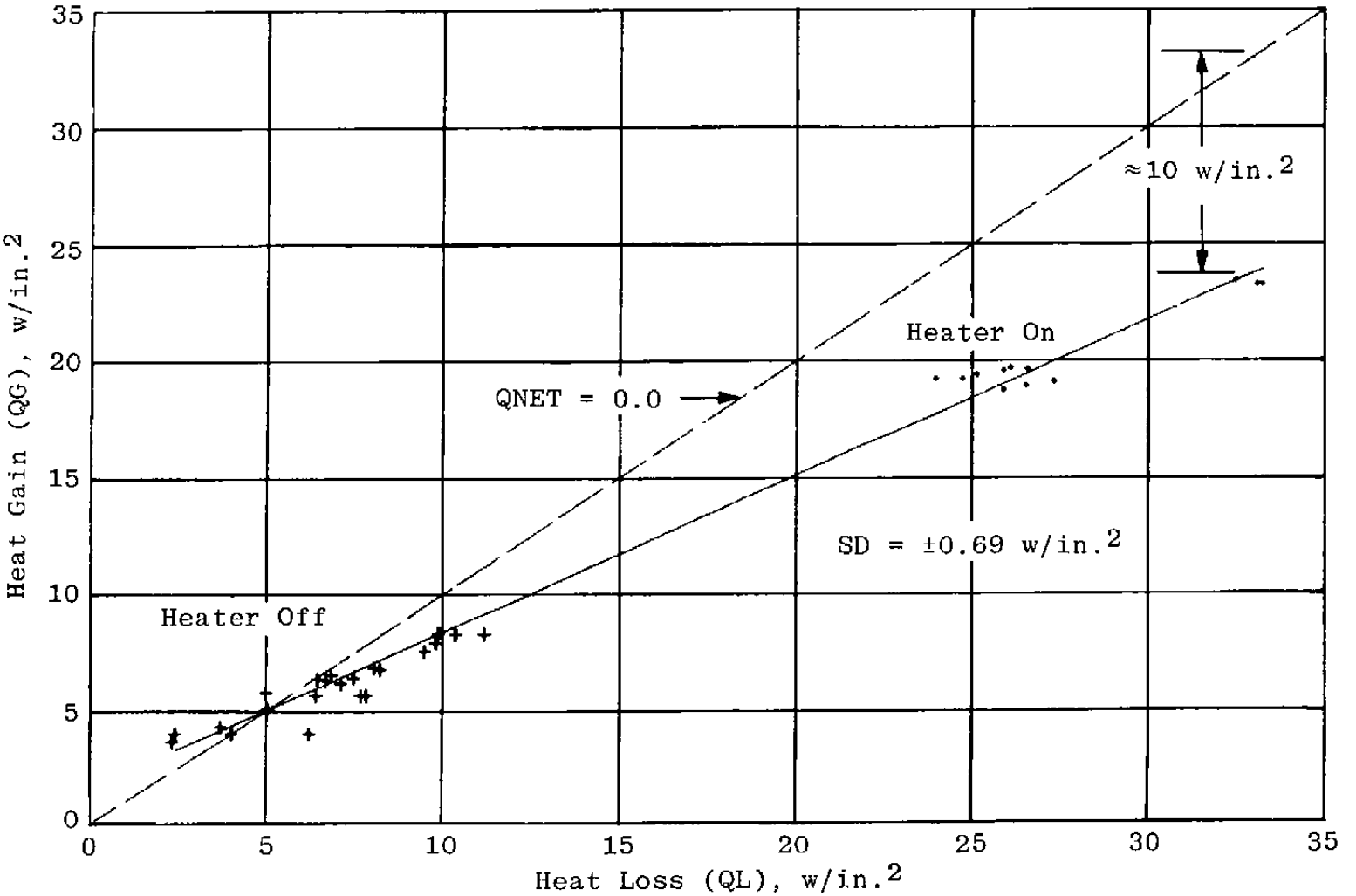

Figure 16. Thermal balance, wet air (Configuration B).

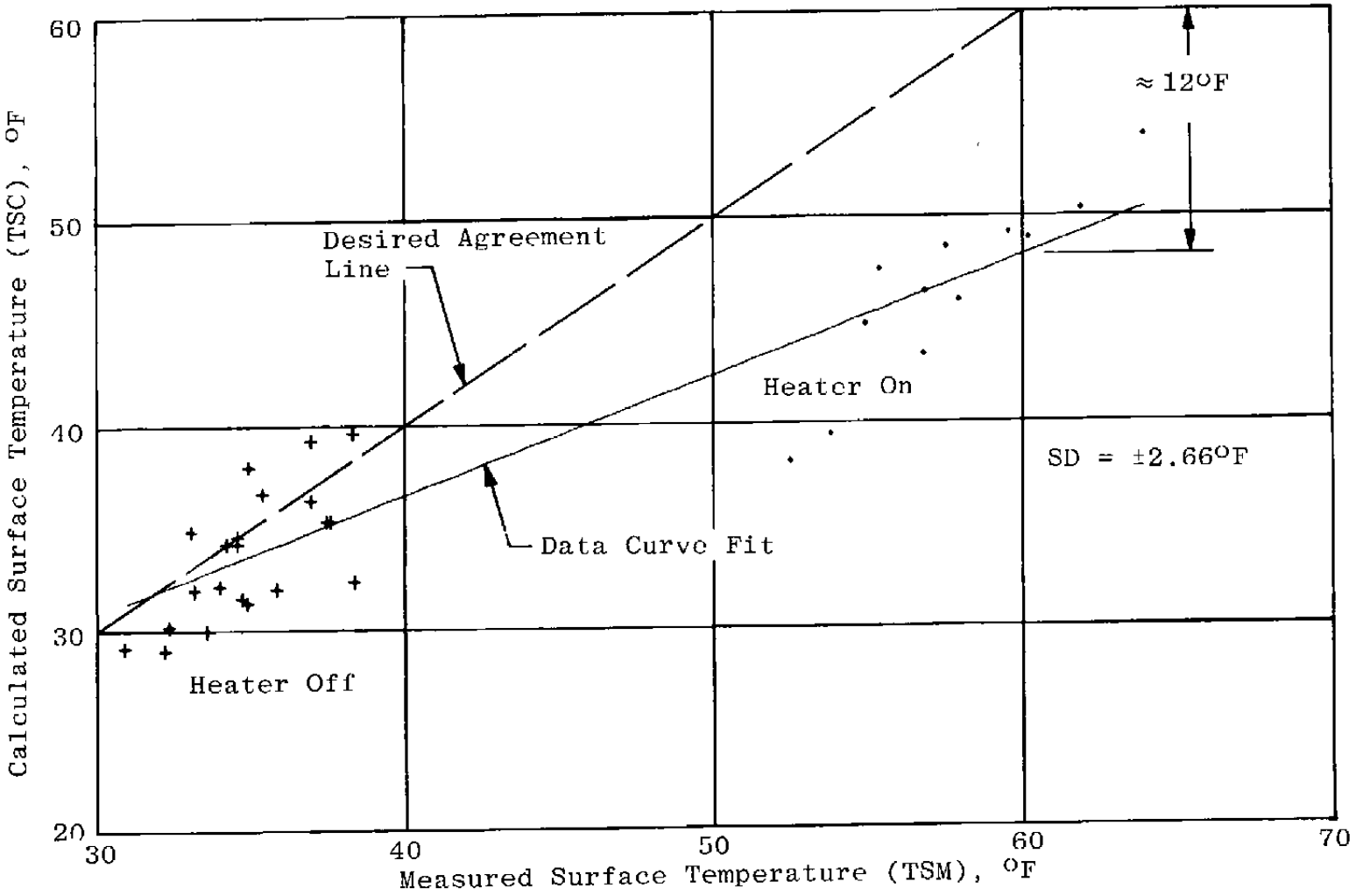

Figure 17. Calculated versus measured surface temperature, wet air (Configuration B).

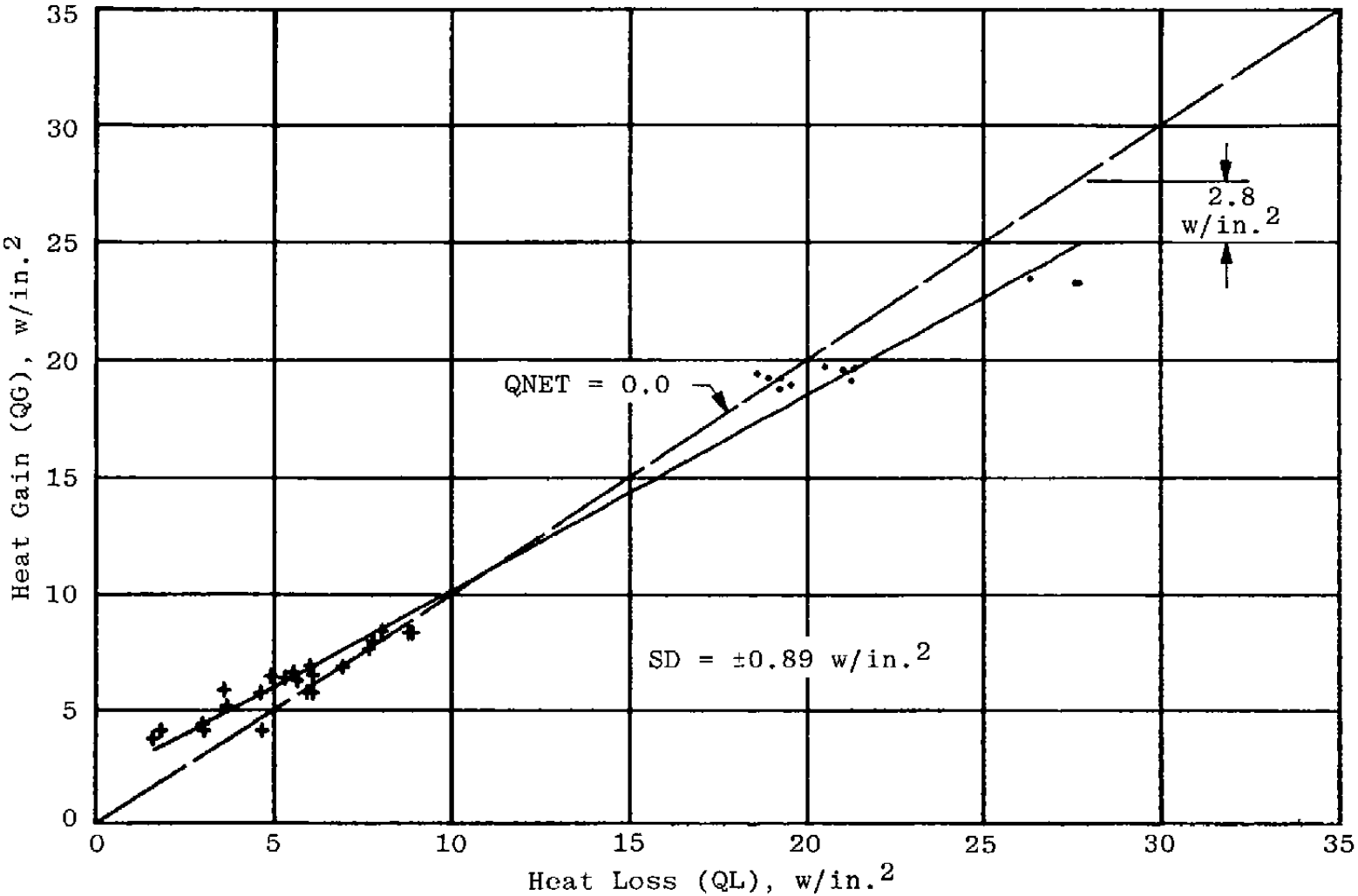

Figure 18. Thermal balance, model adjusted, wet air (Configuration B).

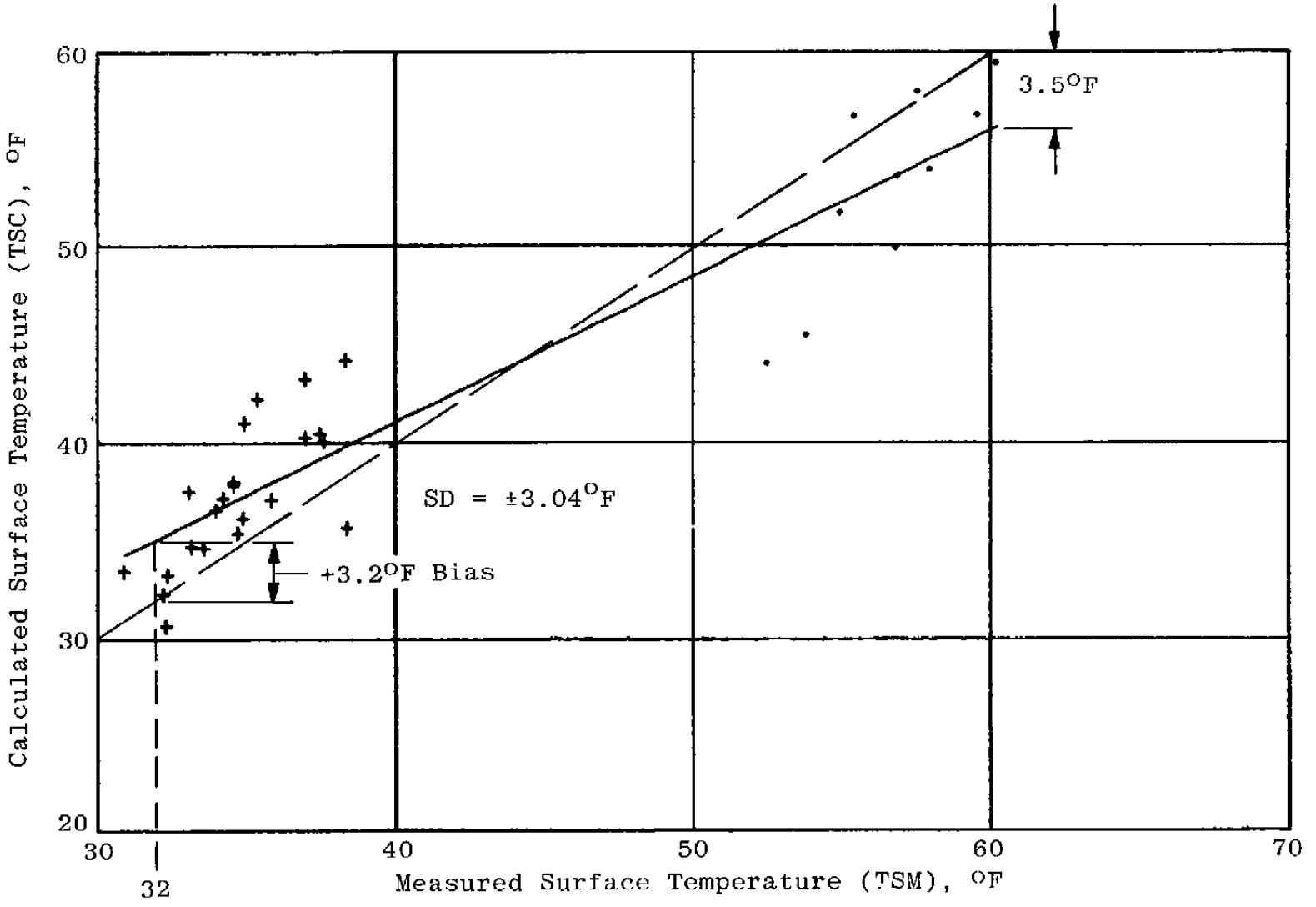

Figure 19. Calculated versus measured surface temperature, model adjusted, wet air (Configuration B).

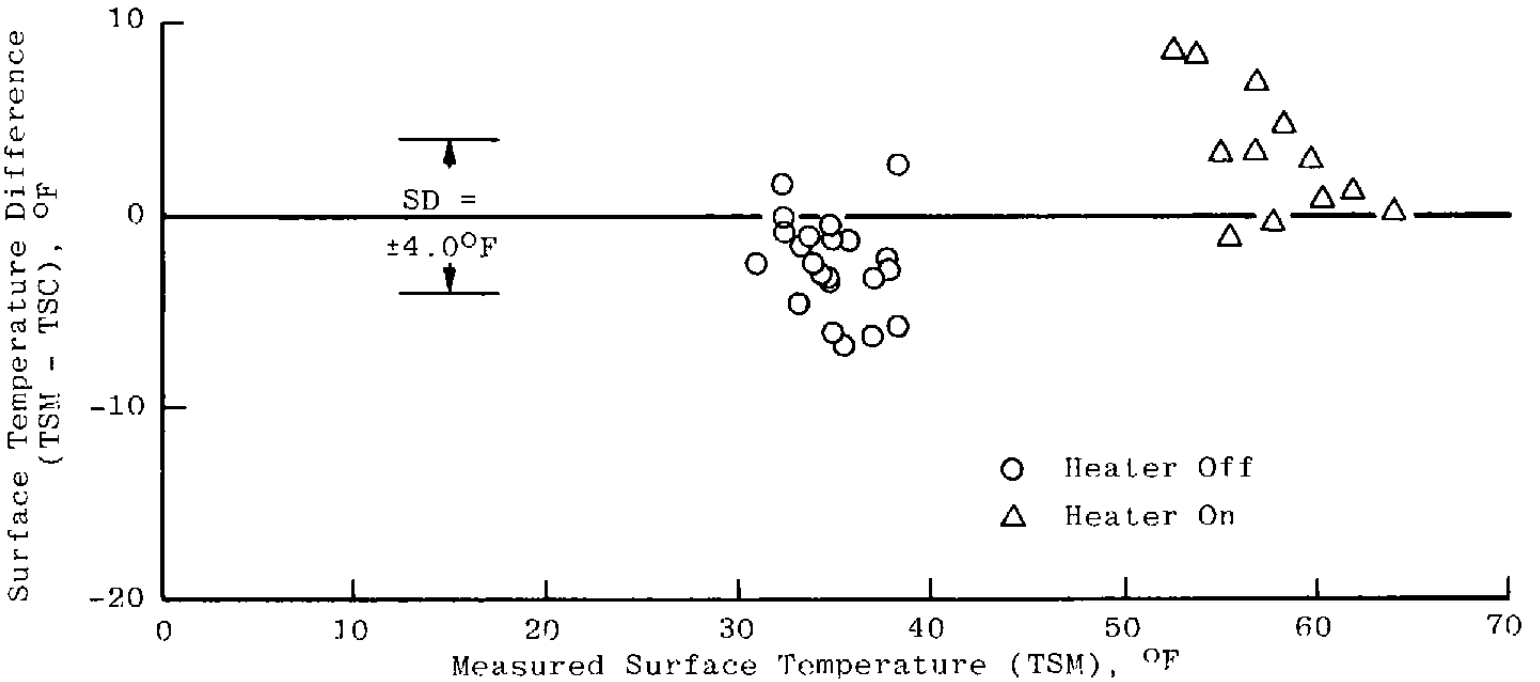

Figure 20. Difference between measured and calculated leading-edge surface temperatures, model adjusted, wet air (Configuration B).

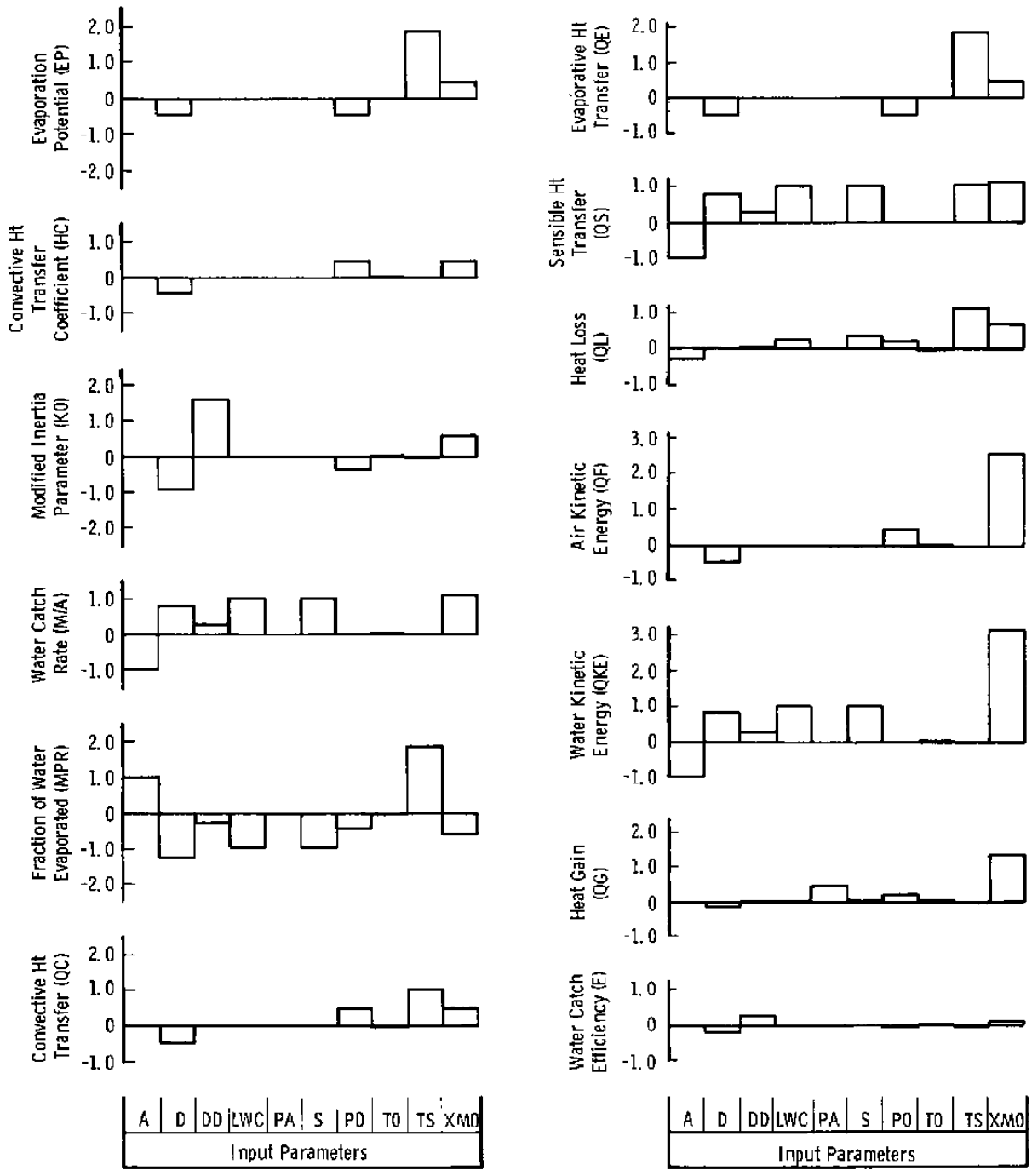

A	Leading-Edge Area	S	Airfoil Span
D	Leading-Edge Effective Diameter	PO	Free-Stream Static Pressure
DD	Droplet Diameter	TO	Free-Stream Static Temperature
LWC	Liquid Water Content	TS	Leading-Edge Surface Temperature
PA	Heater Power Density	XMO	Flight Mach Number

Figure 21. Sensitivity of output parameters for a one-percent increase in input parameters.

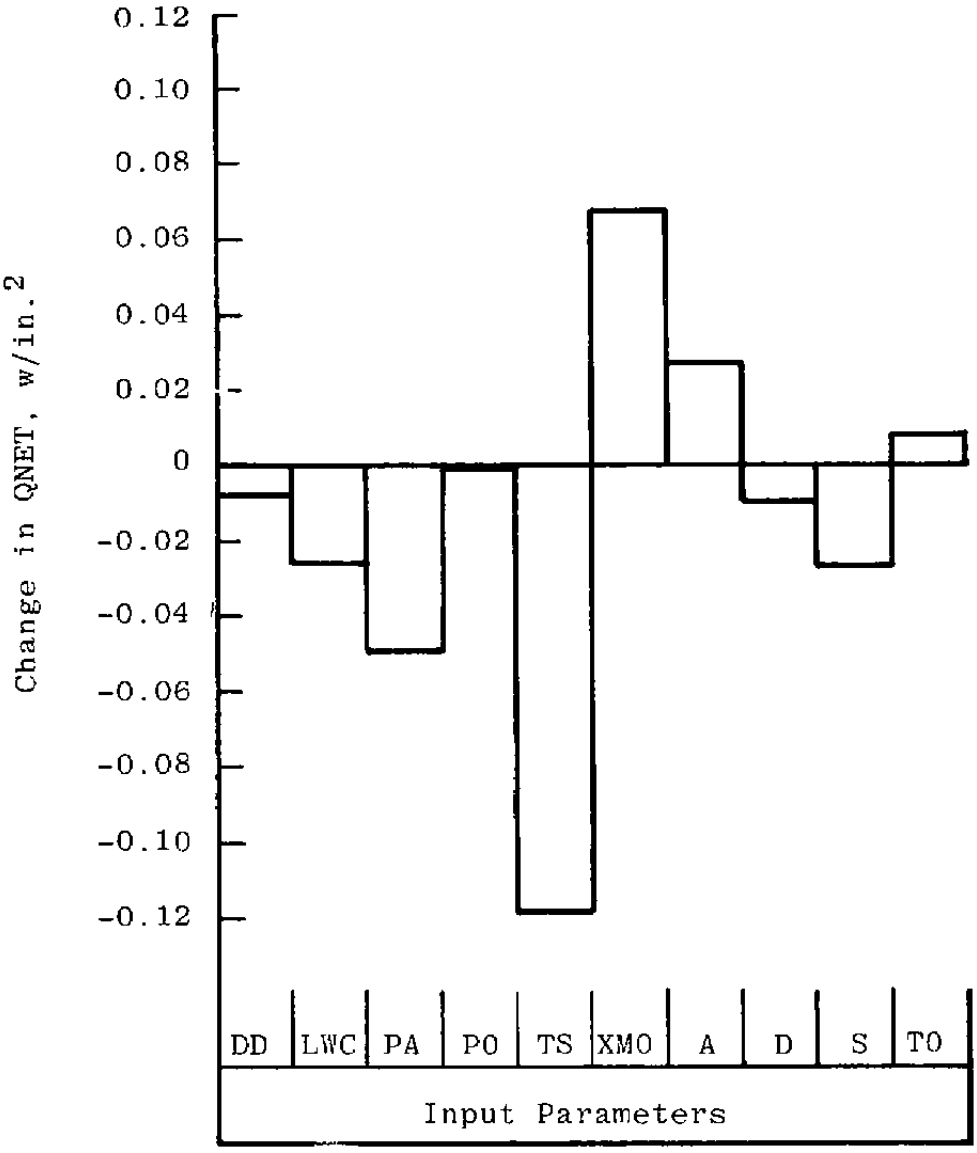

Figure 22. Sensitivity of QNET for a one-percent increase in input parameters.

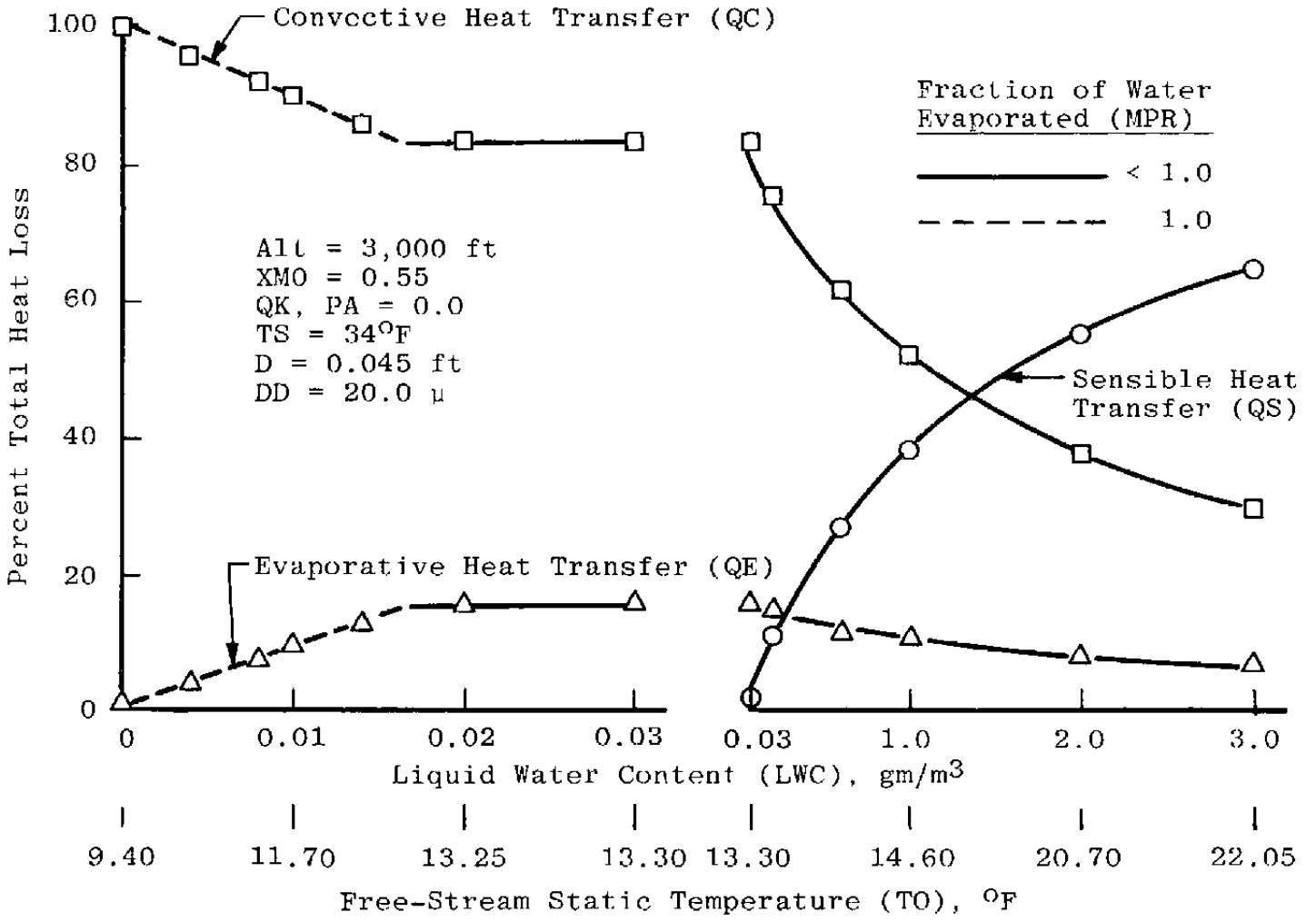

Figure 23. Typical heat loss audit as a function of liquid water content.

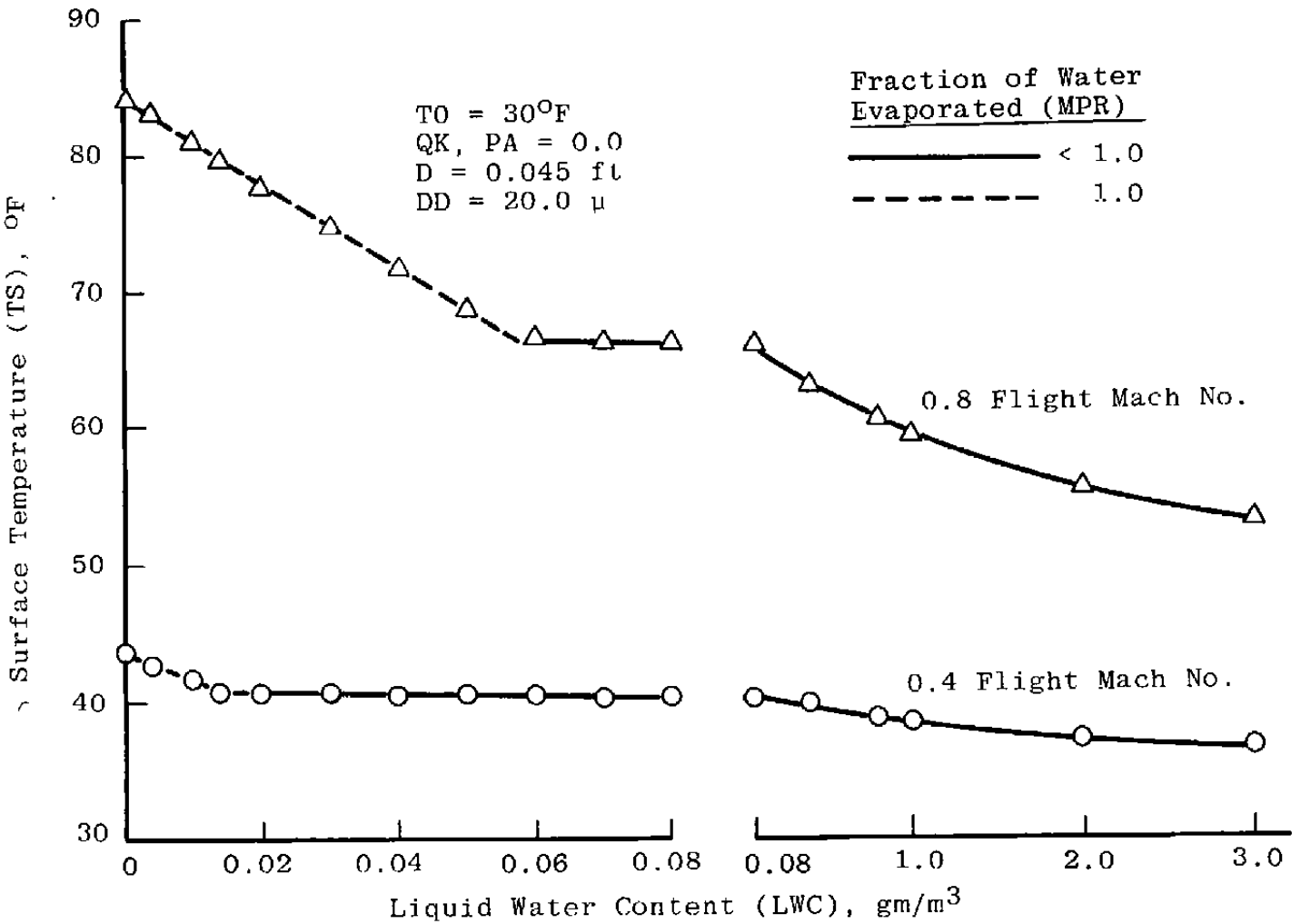

a. 3,000-ft altitude

Figure 24. Effect of liquid water content on leading-edge surface temperature.

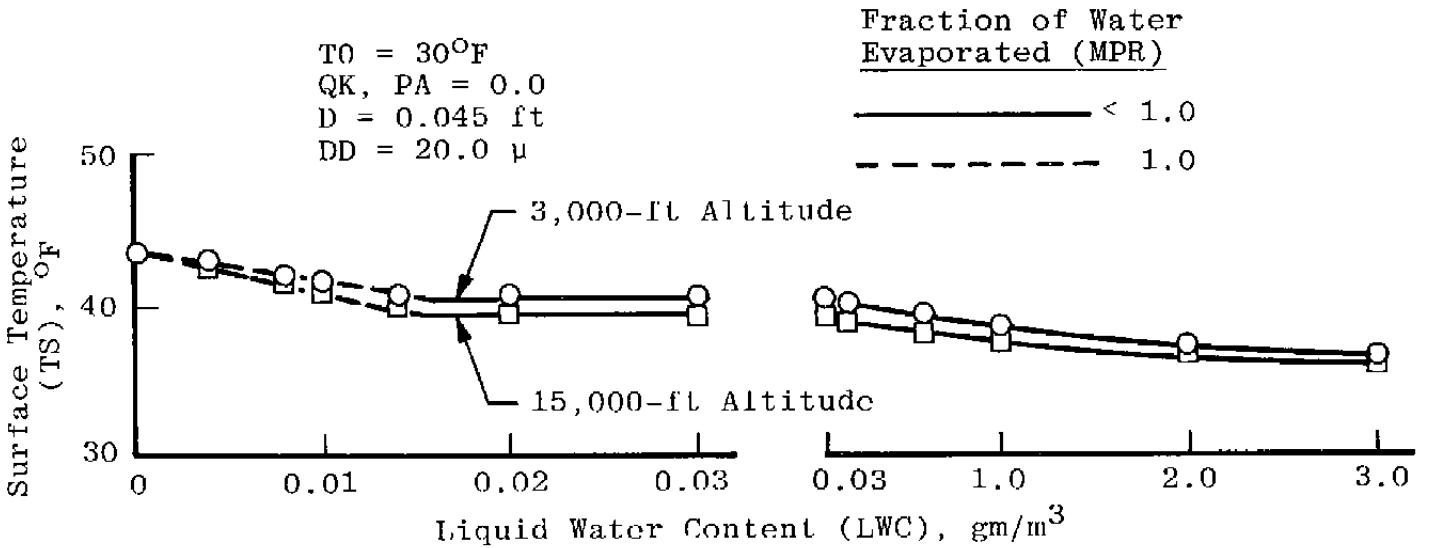

b. 0.4 Flight Mach No.

Figure 24. Concluded.

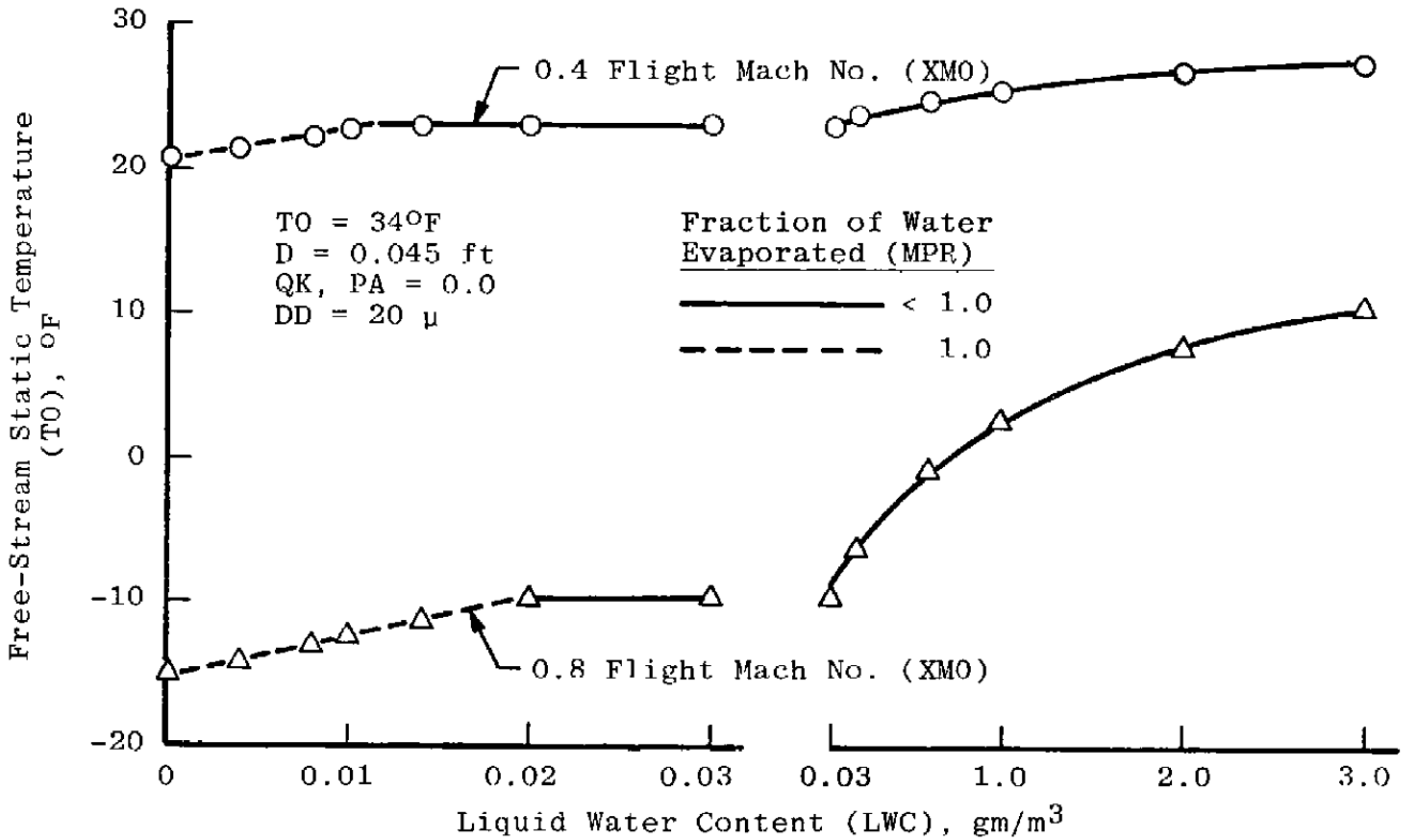

a. 3,000-ft altitude

Figure 25. Effect of liquid water content on free-stream static temperature.

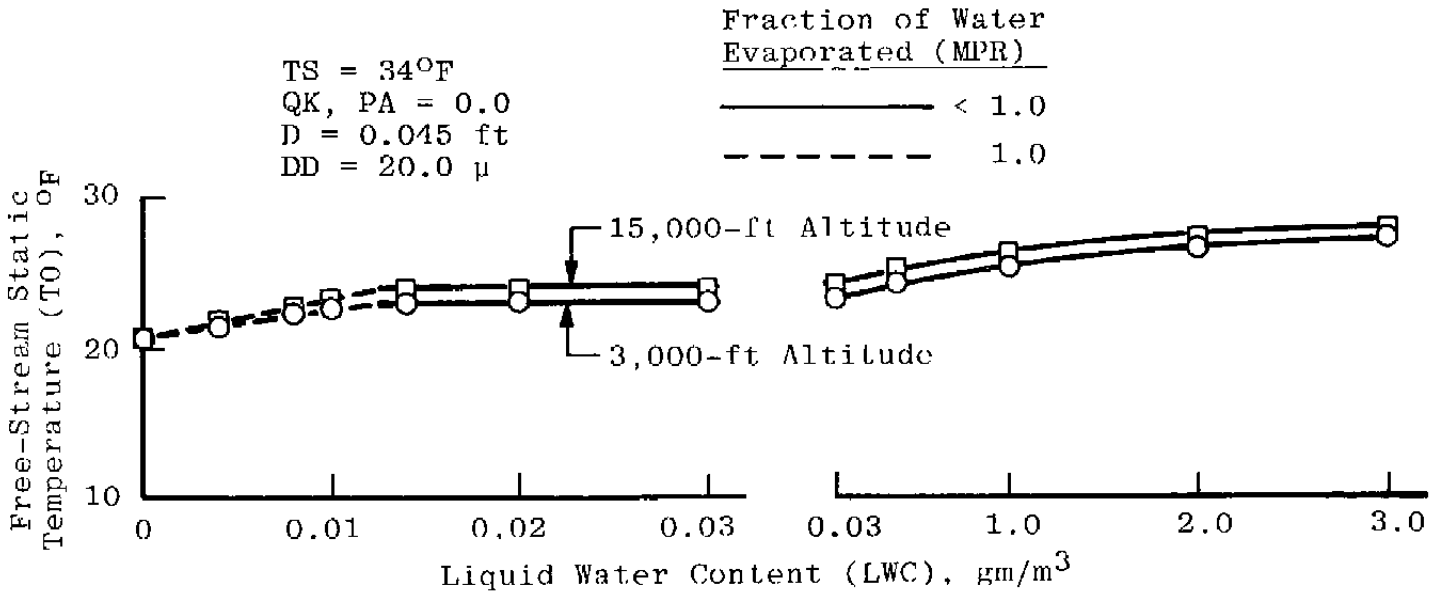

b. 0.4 Flight Mach No.

Figure 25. Concluded.

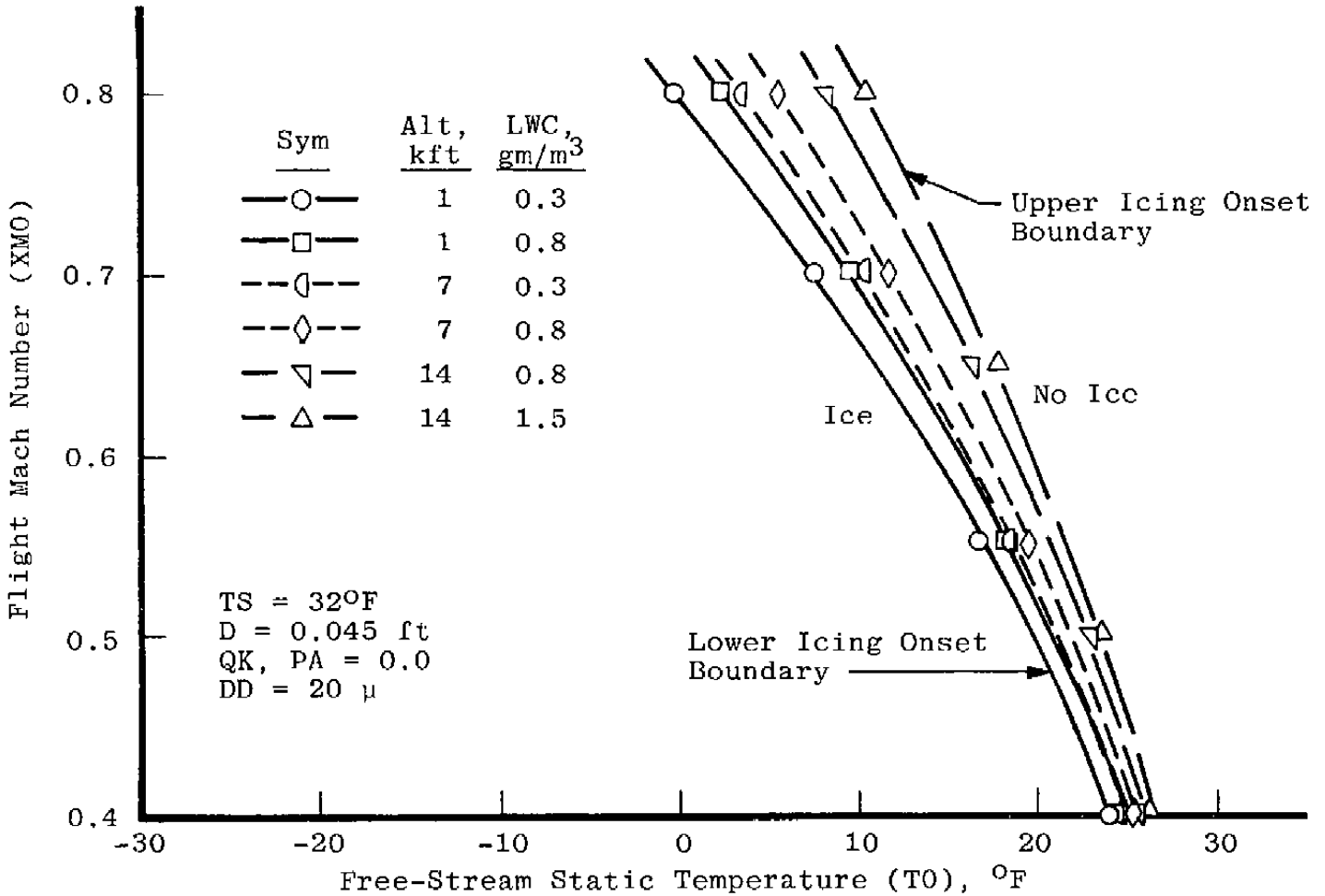

Figure 26. Icing onset predictions, isolated airfoil (Configuration B).

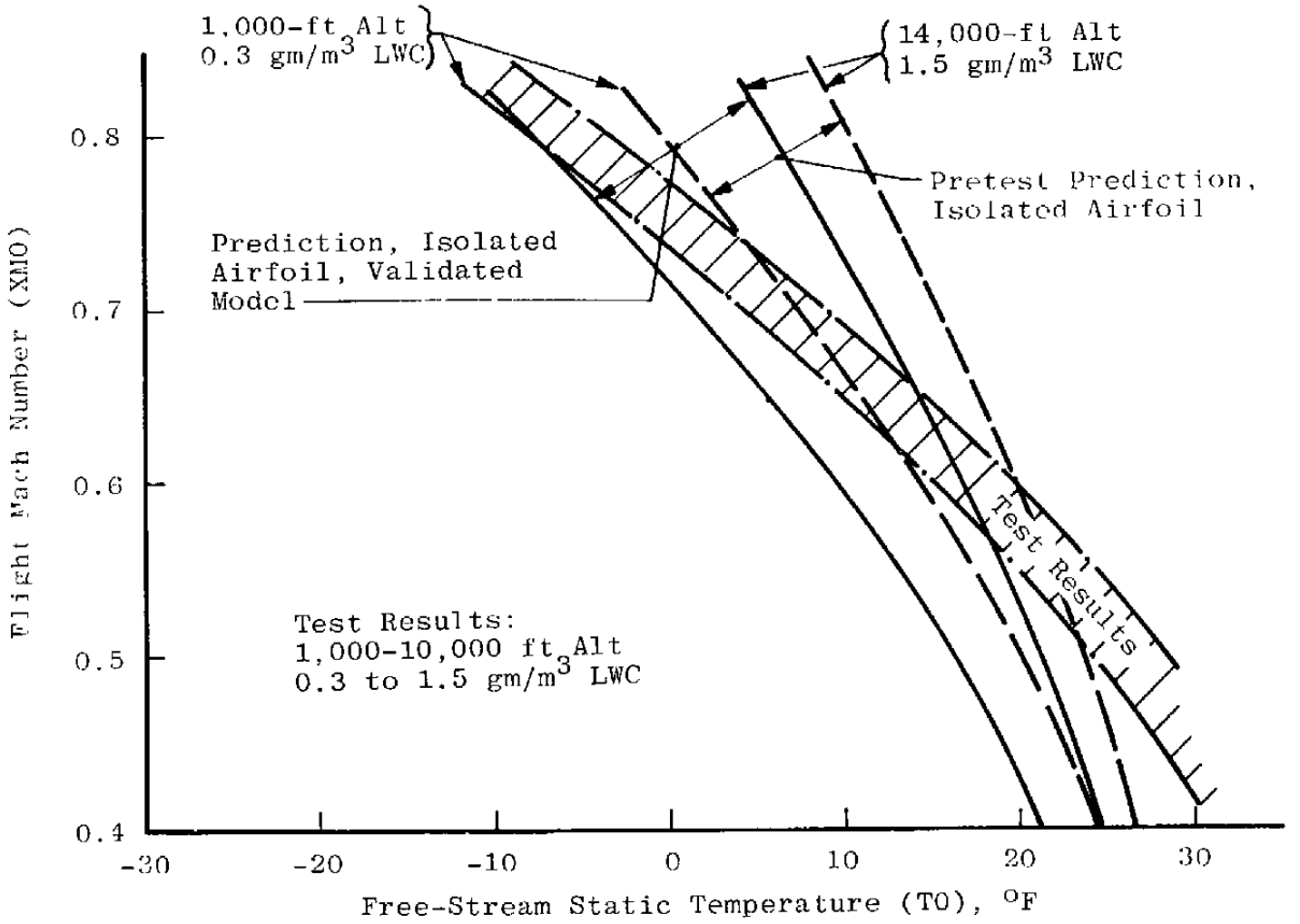

Figure 27. Comparison of icing onset predictions and test results (Configuration B).

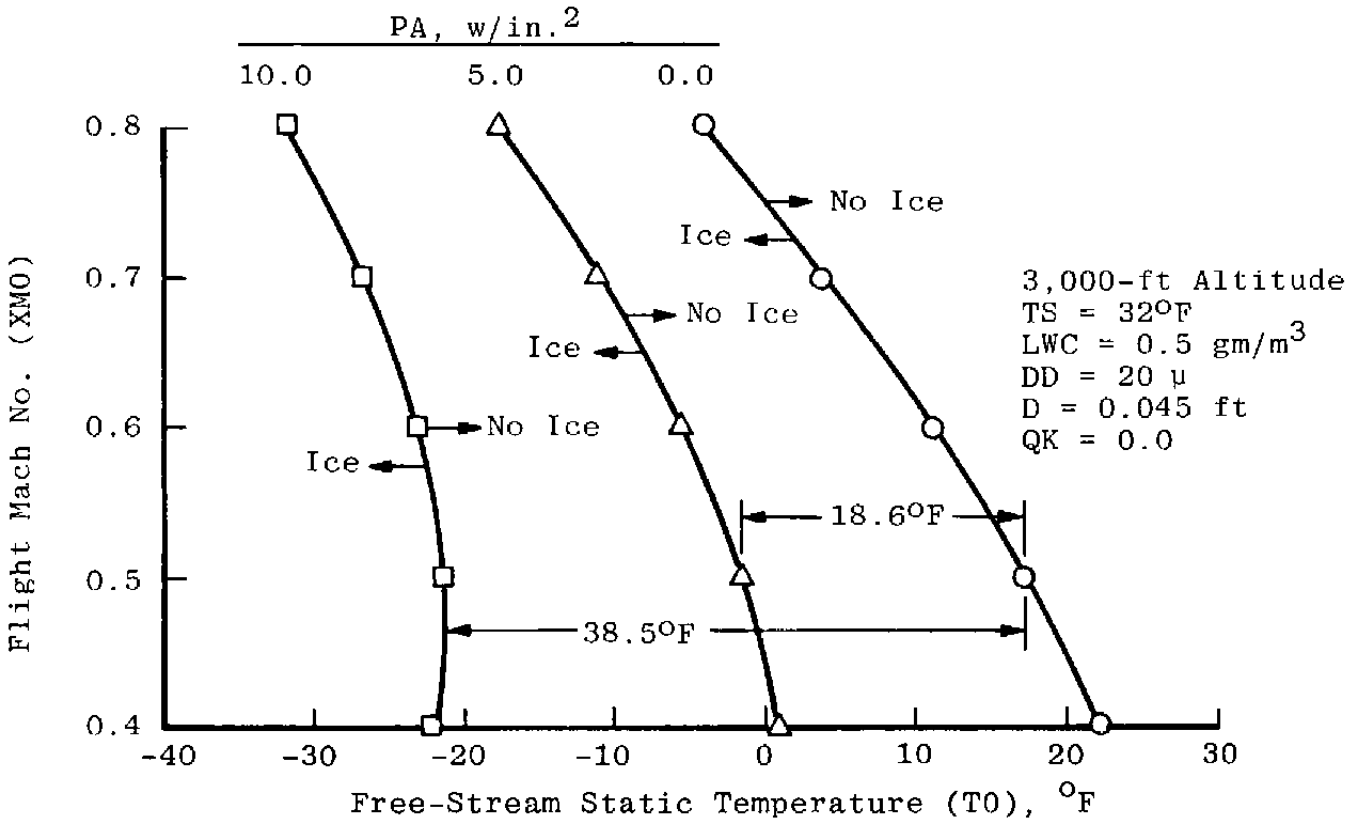

Figure 28. Effect of heater on reducing icing onset temperature.

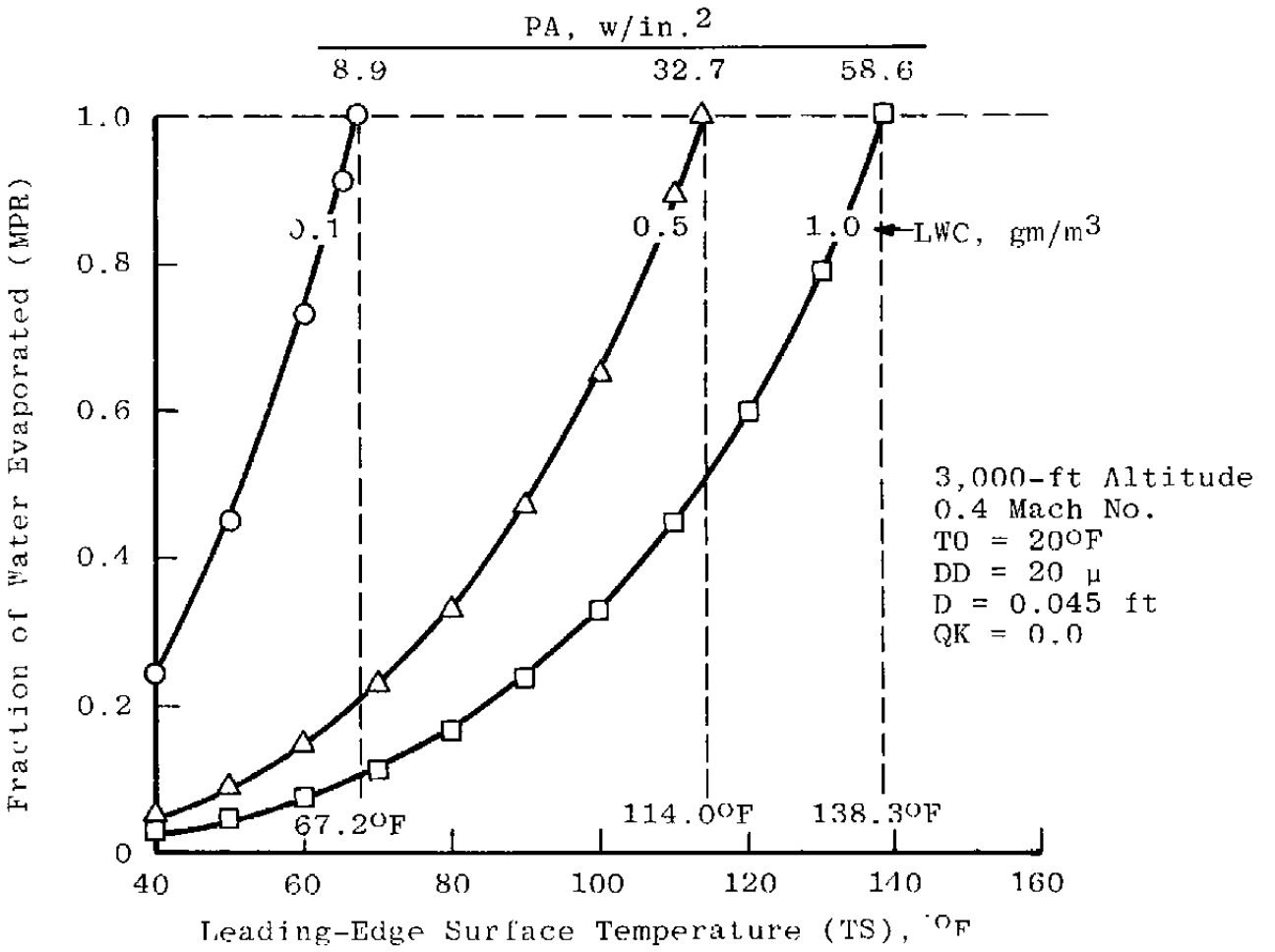

Figure 29. Surface temperature and power density required for dry anti-icing.

Table 1. Uncertainties of Calculated Data

3,000-ft Altitude, 0.55 Mach No., 0.8-gm/m^3 Liquid Water Content

Data	Uncertainty, Heat Gain (QG), percent	Uncertainty, Heat Loss (QL), percent
Configuration A	4.72	9.05
Configuration B	7.60	5.25

Table 2. Model Sensitivity for a One-Percent Increase in Input Parameters

Input Parameter	Parameter Units	Base Values	1-percent Increase In Input Parameter	Output Parameter														
				E	EP	HC	K0	M/A	MPR	QC	QE	QS	QL	QF	QKE	QG	QNET	QNET Change, w/in.^{2}
				Base Values														
				0.7953	1.4279, lbm/hr-ft^2	92.5707, Btu/hr-ft	3.9709	53.6781, lbm/hr-ft^2	0.0266	5.9770, w/in.^{2}	0.9241, w/in.^{2}	3.4355, w/in.^{2}	10.3365, w/in.^{2}	4.6081, w/in.^{2}	0.7329, w/in.^{2}	10.3410, w/in.^{2}	0.0044, w/in.^{2}	
				Percent Change in Output Parameter														
DD	m	20.00	20.20	0.2957	0	0	1.6047	0.2957	−0.2948	0	0	0.2957	0.0983	0	0.2957	0.0210	−180.7	8.0080
LWC	gm/m^3	0.80	0.808	0	0	0	0	1.0001	−0.9901	0	0	1.0000	0.3324	0	1.0000	0.0709	−611.3	−0.0270
PA	w/in.^{2}	5.00	5.05	0	0	0	0	0	0	0	0	0	0	0	0	0.4835	1130.9	−0.0500
P0	psia	13.171	13.30	−0.0745	−0.4962	0.4988	−0.3971	−0.0744	−0.4221	0.4988	−0.4963	−0.0745	0.2193	0.4987	−0.0744	0.2170	−5.2631	0.0002
TS	°F	34.00	34.34	−0.0004	1.8609	−0.0004	−0.0022	−0.0003	1.8612	1.0802	0.8608	1.0802	0.1500	−0.0004	−0.0004	−0.0082	−2689.1	−0.1189
XM0	—	0.55	0.5555	0.1113	0.4989	0.4988	0.5988	1.1125	0.6064	0.4988	0.4988	1.112	0.7027	2.5188	3.1449	1.3453	1503.6	0.0665
A	ft^2	0.16	0.1616	0	0	0	0	−0.9901	1.0000	0	0	−0.9901	−0.3291	0	−0.9901	−0.0702	605.22	0.0268
D	ft	0.045	0.04545	−0.1869	−0.4961	−0.4962	−0.9901	0.8112	−1.2968	−0.4963	−0.4962	0.8112	−0.0617	−0.4963	0.8112	−0.1637	−238.57	−0.0105
S	ft	2.30	2.323	0	0	0	0	1.0001	−0.9901	0	0	1.0000	0.3324	0	1.0001	0.0709	−611.28	−0.0270
T0	°F	2.55	2.5755	0.0002	−0.0398	0.0014	0.0018	0.0030	−0.0429	−0.0801	−0.0399	−0.0785	−0.0760	0.0069	0.0086	0.0037	186.24	0.0082

Note: Alt = 3,000 ft; Mach number = 0.55

NOMENCLATURE

A	Leading-edge surface area, ft^2
A0, A1	First-order curve-fit coefficients
ALT	Geopotential altitude, ft
CA	Specific heat at constant pressure for air, Btu/lbm-°F
CW	Specific heat of water, Btu/lbm-°F
D	Leading-edge thickness or effective diameter, in., ft
DD	Volume median water droplet diameter, μ (microns)
DF	Diffusion coefficient, ft^2/hr
DT	Interface temperature gradient, °F
E	Water catch efficiency
EC	Evaporative correlation coefficient
EP	Evaporation potential, $lbm/hr\text{-}ft^2$
G	Constant, 32.174 $lbm\text{-}ft/lbf\text{-}sec^2$
HC	Calculated convective heat-transfer coefficient, $Btu/hr\text{-}ft^2\text{-}°F$
HT	Heat
I	Dimensionless parameter
J	Mechanical equivalent of heat, 778 ft-lbf/Btu
K	1,000; also conduction heat-transfer coefficient, Btu/hr-ft-°F
KM	Mass transfer function, lbm-°F/Btu

K0	Modified inertia parameter
L	Latent heat of vaporization for water, Btu/lbm
LWC	Liquid water content, gm/m^3
M	Water catch rate, lbm/hr
M/A	Water catch rate per unit area, $lbm/hr\text{-}ft^2$
MPR	Fraction of water evaporated
MU	Air viscosity, $lbf\text{-}sec/ft^2$
PA	Heater power density, $Btu/hr\text{-}ft^2$, $w/in.^2$
P0	Free-stream static pressure (ambient), psia
PR	Prandtl number
PT0	Free-stream total pressure, psia
PT0W	Water vapor pressure at T0, psia
PTSW	Water vapor pressure at TS, psia
QC	Convective heat transfer, $Btu/hr\text{-}ft^2$, $w/in.^2$
QE	Evaporative heat transfer, $Btu/hr\text{-}ft^2$, $w/in.^2$
QF	Air kinetic energy, $Btu/hr\text{-}ft^2$, $w/in.^2$
QG	Heat gain, sum of QF, QKE, and PA, $Btu/hr\text{-}ft^2$, $w/in.^2$
QK	Conductive heat transfer, $Btu/hr\text{-}ft^2$, $w/in.^2$
QKE	Water kinetic energy, $Btu/hr\text{-}ft^2$, $w/in.^2$
QL	Heat loss, sum of QC, QE, QS, QK, $Btu/hr\text{-}ft^2$, $w/in.^2$

QNET	Net heat transfer, QG − QL, BTU/hr-ft^2, w/in.^{2}
QS	Sensible heat transfer, Btu/hr-ft^2, w/in.^{2}
R	Boundary-layer recovery factor
RHO	Air density, lbm/ft^3
S	Airfoil span (inlet perimeter), ft
SC	Schmidt number
SD	Estimate of the one-sigma standard deviation
T1, 2, etc.	Temperature, °F
TF	Reference temperature, °R
TFK	Reference temperature, °K
T0	Free-stream static temperature (ambient), °F
TT0	Free-stream total temperature, °F, °R
TS	Leading-edge surface temperature, °F, °R
TSC	Calculated surface temperature, °F
TSM	Measured surface temperature, °F
V	Flight velocity, ft/sec
VK	Flight velocity, knots
X	Average thickness of structural interface, ft
XM0	Flight Mach number